Very Fast Electron Migrations within p-Doped Aromatic Cofacial Arrays Leading to Three-Dimensional (Toroidal) π-Delocalization

Sergiy V. Rosokha, Ivan S. Neretin, Duoli Sun, and Jay K. Kochi*

Contribution from the Department of Chemistry, University of Houston, Houston, Texas 77204-5003

Received January 19, 2006; E-mail: jkochi@uh.edu

Abstract: The *charge-resonance* phenomenon originally identified by Badger and Brocklehurst lies at the core of the basic understanding of electron movement and delocalization that is possible within p-doped aromatic (face-to-face) arrays. To this end, we now utilize a series of different aryl-donor groups (Ar) around a central platform to precisely evaluate the intramolecular electron movement among these tethered redox centers. As such, the unique charge-resonance (intervalence) absorption bands observed upon the one-electron oxidation or p-doping of various hexaarylbenzenoid arrays (Ar_6C_6) provide quantitative measures of the reorganization energy (λ) and the electronic coupling element (H_{ab}) that are required for the evaluation of the activation barrier (ΔG_{ET}^*) for electron-transfer self-exchange according to Marcus−Hush theory. The extensive search for viable redox centers is considerably aided by the application of a voltammetric criterion that has led in this study to Ar = *N,N*-dialkyl-*p*-anilinyl, in which exceptionally low barriers are shown to lie in the range $\Delta G_{ET}^* = 0.3-0.7$ kcal mol^{-1} for very fast electron hopping or peregrination around the hexagonal circuit among six equivalent Ar sites. Therefore, at transition temperatures $T_t > 0.5/R$ or roughly −20 °C, the electron-transfer dynamics become essentially barrierless since the whizzing occurs beyond the continuum of states and effectively achieves *complete π-delocalization*.

Introduction

The efficient (three-dimensional) delocalization of electrons within extended organic arrays represents an emerging research frontier for various novel applications of fullerenes, nanotubes, and Mobius systems.[1] Electron delocalizations in such aromatic structures mostly occur in relatively thin surface layers, and the development of new topologies that allow broad three-dimensional delocalization constitutes a fascinating synthetic challenge.[2] Another promising but conceptually different approach to this problem derives from through-space electron delocalization in open-shell (p-doped) systems consisting of planar aromatic donors (ArH) and their cofacial cation-radical counterparts (ArH•+), as schematically depicted in Chart 1 (for ArH = C_6H_6), where the blue arrows represent the odd-electron (or positive charge) movement between the juxtaposed π-faces.[3] Such an electron interchange within the cationic $(ArH)_2^{•+}$ complex is modulated by the electronic coupling element (H_{ab}),

Chart 1

so that strong coupling results in complete π-delocalization of positive charge, and a weaker coupling leads to electron hopping between the intermolecular aromatic sites.[4] As such, π-delocalization has been experimentally observed in dimeric cation-radicals of naphthalene, octamethylbiphenylene, phenalenyl, etc.,[5] whereas electron hopping has been reported for the dimeric cation-radicals of dimethoxybenzenes, phenothiazines, and tetrathiafulvalene,[6] as well as in dimeric anion-radicals of tetracyanoethylene, chloranil, and dinitrobenzene.[7] From the

(1) For a recent thematic issue on σ- and π-delocalization, see: Schleyer, P. v. R., Guest Ed. *Chem. Rev.* **2005**, *105*, 3433.
(2) (a) Chen, Z.; King, R. B. *Chem. Rev.* **2005**, *105,* 3613. (b) Lu, X.; Chen, Z. *Chem. Rev.* **2005**, *105*, 3643. (c) Rzepa, H. S. *Chem. Rev.* **2005**, *105*, 3697.
(3) (a) This represents the prototypical first (dyad) member of a wide variety of p-doped aromatic arrays. For some specific examples of p-doped cofacial dyads, see: (b) Meot-Ner, M.; Hamlet, P.; Hunter, E. P.; Field, F. H. *J. Am. Chem. Soc.* **1978**, *100*, 5466. (c) Meot-Ner, M. *J. Phys. Chem.* **1980**, *84*, 2724. (d) Meot-Ner, M.; El-Shall, M. S. *J. Am. Chem. Soc.* **1986**, *108*, 4386. (e) Masnovi, J. M.; Kochi, J. K. *J. Phys. Chem.* **1987**, *91,* 1878. (f) Rathore, R.; Abdelwahed, S. H.; Guzei, I. A. *J. Am. Chem. Soc.* **2003**, *125*, 8712. (g) For more general examples of p-doping, see: Cox P. A. *The Electronic Structure and Chemistry of Solids*; Oxford University Press: New York, 1987.

(4) The potential-energy surface for an electron-hopping process (via localized adiabatic states) is characterized by the presence of two potential minima with an activation barrier ΔG_{ET}^* for the electron-transfer rate, whereas no such barrier exists for π-delocalization. Experimentally, fast electron hopping can sometimes (but not always) be distinguished by time-resolved spectroscopy — as in the use of temperature-dependent ESR line-broadening techniques with micro- to nanosecond resolution.
(5) (a) Kochi, J. K.; Rathore, R.; Le Magueres, P. *J. Org. Chem.* **2000**, *65*, 6826. (b) LeMagueres, P.; Lindeman, S. V.; Kochi, J. K. *Org. Lett.* **2000**, *2*, 3562. (c) Le Magueres, P.; Lindeman, S.; Kochi, J. K. *J. Chem. Soc., Perkin Trans. 2* **2001**, 1180. (d) Small, D.; Zaitsev, V.; Jung, Y.; Rosokha, S. V.; Head-Gordon, M.; Kochi, J. K. *J. Am. Chem. Soc.* **2004**, *126*, 13850.
(6) (a) Sun, D.; Rosokha, S. V.; Lindeman, S. V.; Kochi, J. K. *J. Am. Chem. Soc.* **2003**, *125*, 15950. (b) Sun, D.; Rosokha, S. V.; Kochi, J. K. *J. Am. Chem. Soc.* **2004**, *126*, 1388. (c) Rosokha, S. V.; Kochi, J. K. Submitted for publication.

standpoint of the classification of classical mixed-valence complexes,[8,9] π-delocalization and electron hopping are distinguished via the Robin−Day paradigm[10] as Class III (delocalized) versus Class II (localized), respectively, such that Class III systems have $H_{ab} > \lambda/2$ and Class II systems have $H_{ab} < \lambda/2$ (where λ is defined as the Marcus reorganization energy).[11]

In solution, the intermolecular π-electron interchange can be experimentally recognized via the distinctive appearance of near-IR absorptions and doubled ESR spectra in dimeric (paramagnetic) π-complexes of p-doped aromatic dyads.[12,13] In the solid state, analogous π-electron interchanges are observed in extended (p-doped) face-to-face arrays containing a large number of π-stacked aromatic donor units as potential molecular "wires" (Chart 2.) These are characterized via their distinctive X-ray

Chart 2

crystallography,[14] and such novel electron-carriers constitute the molecular basis for the construction of unusual organic conducting and magnetic materials.[15] Since the Robin−Day classification has been shown to be applicable to intermolecular (through-space) as well as to intramolecular (through-bond) electron exchange in p-doped aromatic dyads,[6,7] let us now consider discrete examples showing extensive electron interchange involving multiple (yet a *finite* number of) redox centers that would constitute the intermediate bridge between (a) the pairwise interaction in a well-defined [1:1] cation-radical π-complex, as in Chart 1, and (b) the polycentric interactions in an essentially infinite p-doped solid-state stack, as in Chart 2. Indeed, until very recently,[16] there were no extant examples

of extensive (multiple) interchange in which electron or hole migration could be unambiguously demonstrated to take place over more than the requisite minimum number of two aromatic centers in Chart 1.

Basically, the experimental problem of *quantitatively* assessing π-delocalization versus electron hopping between sites in extended systems depends on the proper evaluation of the discrete pairwise dyad as in Chart 1, since the theoretical formulation by Marcus and Sutin[11] has been shown to be applicable to such electron-transfer (donor/acceptor) self-exchange in Robin−Day Class II systems.[6,7,17] To this end, we recognize that a multiple array of aryl-donor groups all tethered around a central platform corresponds to the discrete version of stacked aromatic sites in Chart 2. As such, we examine how hexaarylbenzene structures[18−20] can serve as the prototypical bridge between the discrete dyad (Chart 1) and infinite solid-state (Chart 2) systems in at least two ways: First, when all six aryl-donor groups (D) are equivalent, the electron hopping between hexad sites describes a "closed" loop migration of electronic charge around the central C_6-core, as in **I** (Chart 3).
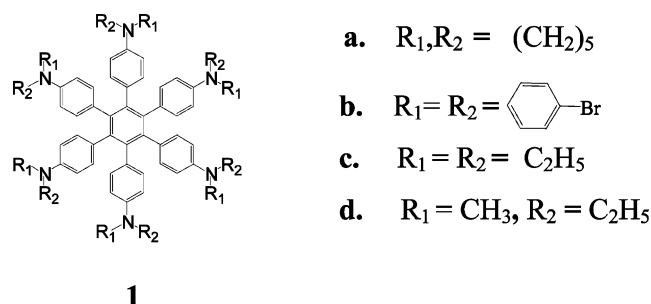
Chart 3
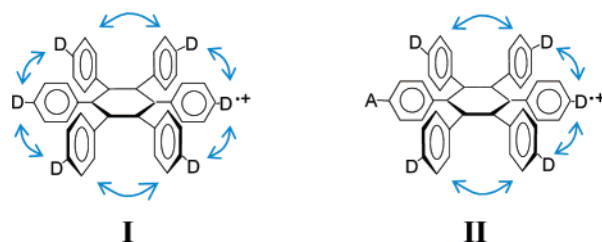
By the same reasoning, the replacement of a single electron donor with an electron-acceptor group (A) interrupts the closed circuit, and electronic migration will then constitute an "open" representative of an abbreviated or finite pentad of cofacial aromatic donor units, as in **II**.

In hexaphenylbenzene and derivatives, the nearly perpendicular arrangement of the six planar substituents relative to the central platform effectively eliminates any through-bridge interactions between these tethered phenyl (aryl) groups.[18b,21]

(7) (a) Ganesan, V.; Rosokha, S. V.; Kochi, J. K. *J. Am. Chem. Soc.* **2003**, *125*, 2559. (b) Rosokha, S. V.; Lu, J.-M.; Newton, M. D.; Kochi, J. K. *J. Am. Chem. Soc.* **2005**, *127*, 7411. (c) Rosokha, S. V.; Newton, M. D.; Head-Gordon, M.; Kochi, J. K. *Chem. Phys.* **2006**, *324*, 117.
(8) (a) Creutz, C. *Prog. Inorg. Chem.* **1983**, *30*, 1. (b) Demadis, K. D.; Hartshorn, C. M.; Meyer, T. J. *Chem. Rev.* **2001**, *101*, 2655. (c) Nishiumi, T.; Nomura, Y.; Chimoto, Y.; Higuchi, M.; Yamamoto, K. *J. Phys. Chem. B* **2004**, *108*, 7992.
(9) (a) Lambert, C.; Nöll, G. *J. Am. Chem. Soc.* **1999**, *121*, 8434. (b) Nelsen, S. F. *Chem. Eur. J.* **2000**, *6*, 581.
(10) Robin, M. B.; Day, P. *Adv. Inorg. Chem. Radiochem*. **1967**, *10*, 247.
(11) (a) Marcus, R. A. *Discuss. Faraday Soc.* **1960**, *29*, 21. (b) Marcus, R. A. *J. Phys. Chem.* **1963**, *67*, 853. (c) Marcus, R. A. *J. Chem. Phys.* **1965**, *43*, 679. (d) Marcus, R. A.; Sutin, N. *Biochim. Biophys. Acta* **1985**, *811*, 265. (e) Sutin, N. *Prog. Inorg. Chem.* **1983**, *30*, 441.
(12) (a) Badger, B.; Brocklehurst, B. *Nature* **1968**, *219*, 263. (b) Badger, B.; Brocklehurst, B. *Trans. Faraday Soc.* **1969**, *65*, 2582; **1970**, *66*, 2939. [These were the first to identify the NIR charge-resonance bands.] (c) Lewis, I. C.; Singer, L. S. *Chem. Phys.* **1965**, *43*, 2712. (d) Howarth, O. W.; Fraenkel, G. K. *J. Am. Chem. Soc.* **1966**, *88*, 4514.
(13) (a) Fritz, H. P.; Gebauer, H.; Friedrich, P.; Ecker, P.; Artes, R.; Schubert, V. *Z. Naturforsch.* **1978**, *336*, 498. (b) Fritz, H. P.; Gebauer, H.; Friederich, F.; Schubert, V. *Angew. Chem.* **1978**, *90*, 305. (c) Enkelmann, V.; Morra, B. S.; Kröhnke, C.; Wegner, G. *Chem. Phys.* **1982**, *66*, 303. (d) Enkelmann, V. *ACS Adv. Chem. Ser.* **1988**, *217*, 177. (d) Herwig, P. T.; Enkelmann, V.; Schmelz, D.; Müllen, K. *Chem. Eur. J.* **2000**, *6*, 1834. (e) Chi, X.; Itkis, M. E.; Reed, R. W.; Oakley, R. T.; Cordes, A. W.; Haddon, R. C. *J. Phys. Chem. B* **2002**, *106*, 8278.
(14) (a) Goldstein, P.; Seff, K.; Trueblood, K. N. *Acta Crystallogr.* **1968**, *B24*, 778. (b) Hanson, A. W. *Acta Crystallogr.* **1968**, *B24*, 773. (c) Kobayashi, H. *Bull. Chem. Soc. Jpn.* **1974**, *47*, 1346. (d) Fourmigue, M.; Perrocheau, V.; Clerac, R.; Coulon, C. *J. Mater. Chem.* **1997**, *7*, 2235. (e) Ballester, L.; Gutierrez, A.; Perpinan, M. F.; Rico, S.; Azcondo, M. T.; Bellito, C. *Inorg. Chem.* **1999**, *38*, 4430.
(15) (a) Williams, J. M. *Organic Superconductors: Synthesis, Structure, Properties and Theory*; Prentice Hall: Englewood Cliffs, NJ, 1992. (b) Farges, J.-P., Ed. *Organic Conductors: Fundamentals and Applications*; Marcel Dekker: New York, 1994. (c) Miller, J. S., Drillon, M., Eds. *Magnetism: Molecules to Materials*; Wiley-VCH: Weinheim, 2001. (d) See also: Batail. P., Guest Ed. *Chem. Rev.* **2004**, *104*, 4887 (thematic issue).
(16) For a preliminary (in part) report, see: Sun, D.; Rosokha, S. V.; Kochi, J. K. *Angew. Chem.* **2005**, *44*, 5133.
(17) Strictly speaking, two-state theory requires diabatic states in which through-space (aromatic) interchange will involve little π-orbital overlap. The extent of the latter in Ar/Ar$^{\bullet+}$ dyads is roughly limited by the π-separation, and previous studies showed that, at the van der Waals distance of $r_{vdW} \approx 3.4$ Å, the π-overlap can be neglected in the semiquantitative application of the theoretical model.[6,7] Moreover, Mulliken−Hush theory based on the same two-state model leads to values of the electronic coupling element (H_{ab}) which are close to those calculated by ab initio molecular orbital analysis.[6c,7c,17b] (b) See ref 6c and Huang, J.-S.; Kertesz, M. *J. Chem. Phys.* **2005**, *122*, 234707.
(18) (a) Lambert, C.; Nöll, G. *Angew. Chem., Int. Ed.* **1998**, *37*, 2107. (b) Lambert, C.; Nöll, G. *Chem. Eur. J.* **2002**, *8*, 3467. (c) Lambert, C. *Angew. Chem., Int. Ed.* **2005**, *44*, 7337.
(19) (a) Kobayashi, K.; Shirasaka, T.; Sato, A.; Horn, E.; Furukawa, N. *Angew. Chem., Int. Ed.* **1999**, *38*, 3483. (b) Bauer, R. E.; Enkelmann, V.; Wiesler, U. M.; Berresheim, A. J.; Müllen, K. *Chem. Eur. J.* **2002**, *8*, 3858. (c) Kobayashi, K.; Sato, A.; Sakamoto, S.; Yamaguchi, K. *J. Am. Chem. Soc.* **2003**, *125*, 3035.
(20) (a) Dijkstra, H. P.; Steenwinkel, P.; Grove, D. M.; Lutz, M.; Spek, A. L.; van Koten, G. *Angew. Chem., Int. Ed.* **1999**, *38*, 2186. (b) Rathore, R.; Burns, C. L.; Deselnicu, M. I. *Org. Lett.* **2001**, *3*, 2887. (c) Traber, B.; Wolff, J. J.; Rominger, F.; Oeser, T.; Gleiter, R.; Goebel, M.; Wortmann, R. *Chem. Eur. J.* **2004**, *10*, 1227. (d) Shen, X.; Ho, D. M.; Pascal, R. A., Jr. *J. Am. Chem. Soc.* **2004**, *126*, 5798. (e) Rathore, R.; Burns, C. L.; Abdelwahed, S. A. **2004**, *6*, 1689. (f) Bottari, G.; Torres, T. *Chem. Comm.* **2004**, 2668. (g) Ito, S.; Ando, M.; Nomura, A.; Morita, N.; Kabuto, C.; Mukai, H.; Ohta, K.; Kawakami, J.; Yoshizawa, A.; Tajiri, A. *J. Org. Chem.* **2005**, *70*, 3939.
(21) Compare: Rosokha, S. V.; Sun, D.; Kochi, J. K. *J. Phys. Chem. A* **2002**, *106*, 2283.

As a result, the optical transitions and electron transfers that may characterize any p-doped hexaarylbenzene and derivatives in Chart 3 will derive from through-space interactions that are equivalent to those extant intermolecularly between neighboring aromatic moieties in Charts 1 and 2.[22] Most importantly, the six aryl groups (with Ar = D-C$_6$H$_4$ in **I**) are sufficient to make this closed hexad array structurally and electronically akin to open vertical stacks of six D-C$_6$H$_5$ donors, thereby eliminating the boundary conditions and alleviating the computational task. Accordingly, we first directed our attention to the synthesis of a series of hexaphenylbenzene derivatives, **1a**−**d**, in which the same nitrogen-centered donor substituent occupies every para position, as shown in Chart 4. In addition to these *N,N*-dialkyl-

Chart 4

a. R$_1$,R$_2$ = (CH$_2$)$_5$

b. R$_1$= R$_2$ = ⟨⟩—Br

c. R$_1$ = R$_2$ = C$_2$H$_5$

d. R$_1$ = CH$_3$, R$_2$ = C$_2$H$_5$

1

and *N,N*-diarylanilinyl derivatives, we also examined the all-heterocyclic analogues, hexakis(*N*-3,6-di-*n*-butoxylcarbazolyl)-benzene (**2**) and hexakis(*N*-pyrrolyl)benzene (**3**),[18b,26] shown in Chart 5, to complete the series of hexad donors.
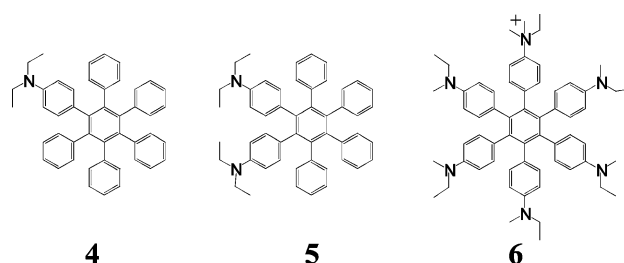
Chart 5

2   **3**
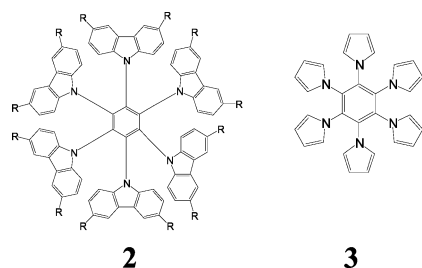
To verify the theoretical analysis (vide infra), we also tested the electronic effects arising from decreasing numbers of interacting donor groups and prepared the monoanilinyl parent **4** and the *ortho*-dianilinyl dyad **5**, together with the open pentad analogue **6** (Chart 6), in which *N*-methylation effectively creates a single ammonium-acceptor center that effectively inhibits full toroidal conjugation.

Results

I. Synthesis and Structural Characterization of Hexaaryl-benzenoid Donors. A. Synthetic Methodologies. The aryl-

(22) (a) Although the dihedral angle between neighboring (cofacial) aromatic groups in hexaarylbenzenes subtends a ∼60° angle, the difference between orbital overlap with that in the cofacial orientation is insufficient to significantly affect the intervalence band.[6]
(23) Biemans, H. A. M.; Zhang, C.; Smith, P.; Kooijman, H.; Smeets, W. J. J.; Spek, A. L.; Meijer, E. W. *J. Org. Chem.* **1996**, *61*, 9012.
(24) (a) Berresheim, A.; Müller, M.; Müllen, K. *Chem. Rev.* **1999**, *99, 1747.* (b) Watson, M. D.; Fechtenkotter, A.; Müllen, K. *Chem. Rev.* **2001**, *101*, 1267.
(25) Vollhardt, K. P. C. *Acc. Chem. Res.* **1977**, *10,* 1.
(26) (a) Pal, M.; Kandu, N. G. *J. Chem. Soc., Perkin Trans. 1* **1996**, *5*, 449. (b) Fieser, L. F. *Organic Experiment*, 1st ed.; Heath: Boston, 1964; p 307.

Chart 6

4   **5**   **6**

amine-based hexanuclear donors in Chart 4 were prepared via the Co$_2$(CO)$_8$-induced trimerization of bis(*N,N*-dialkylanilinyl)-acetylene[24,25] that was previously prepared by the coupling of the appropriate iodoaniline with acetylene in the presence of palladium catalyst.[26] The heterocyclic analogues in Chart 5 were synthesized according to modified literature procedures[23] by the reaction of hexafluorobenzene with the potassium salts of either carbazole or pyrrole. The pentad donor **6** was prepared from hexaanilinylbenzene **1d** by monomethylation with methyl tri-flate. The corresponding dinuclear dyad (**5**) and mononuclear model (**4**) were synthesized via the Diels−Alder addition of tetraphenylcyclopentadienone to the appropriate dianilinyl- or phenylanilinylacetylene, followed by the elimination of CO.[27] The details of the synthetic procedures and donor characterizations are presented in the Experimental Section.

B. Structural Characterization of Hexanuclear Donors. Pale yellow crystals of hexaanilinyl donors **1c** and **1d** suitable for the X-ray crystallographic analysis were isolated by slow removal of dichloromethane from an equimolar mixture with acetonitrile. X-ray structural analysis in Figure 1A,B shows the
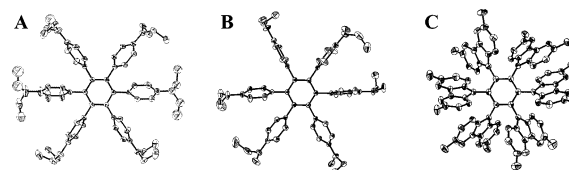
Figure 1. Molecular (ORTEP) structures of hexanuclear donors **1c** (A), **1d** (B), and **2** (C)**,** with hydrogen atoms and solvent molecules, and butyl substituents in **2**, omitted for clarity.

six spoke-like anilinyl groups in a propeller conformation, tilting 72 ± 10° relative to the C$_6$-platform in both hexanuclear donors. All anilinyl moieties retain their benzenoid structure, with ring (C−C) bond lengths of 1.39 ± 0.01 Å and mean planar deviations of less than 0.01 Å. The interplanar dihedral angles between adjoining donor planes are all ∼60°. The distances between adjacent nitrogen centers are uniformly ∼7 Å, and the distance between anilinyl centroids is 4.3 ± 0.3 Å.[28] The central benzenoid ring remains essentially planar and symmetrical, with the aromatic C−C bond length of 1.405 ± 0.005 Å and mean deviation from the plane of 0.007 Å. In a similar way, the X-ray crystal structure of the carbazolyl-based donor **2** (Figure 1C) shows the heteroaromatic planes to be arranged at an angle of 62° relative to the central benzene ring, with distances between nitrogen centers of 2.83 ± 0.03 Å.

II. Voltammetric Characterization of p-Doped Hexaaryl-benzenes. The p-doping of the hexaarylbenzenes depicted in

(27) Tugcu, N.; Park, S. K.; Moore, J. A.; Cramer, S. M. *Ind. Eng. Chem. Res.* **2002**, *41*, 6482.
(28) At this separation, partial solvent penetration at the anilinyl periphery could moderate the electron-transfer process.
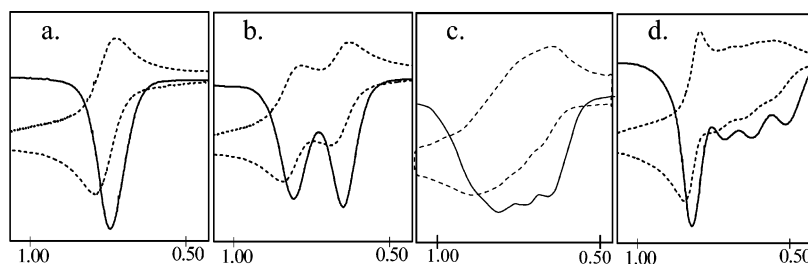
Figure 2. CV (dashed lines) and OSWV (solid lines) voltammograms of the mononuclear donor **4** (a), dinuclear donor **5** (b), pentanuclear donor **6** (c), and hexanuclear donor **1c** (d), showing progressive splittings and potential shifts of the anodic waves with increasing numbers of anilinyl redox centers.

Table 1. Oxidation Potentials of Polynuclear Donors

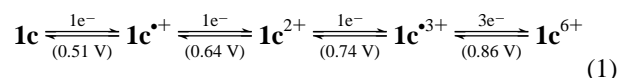| donor	$E_{1/2}$, V vs SCE	ΔE, mV[a]	δE, mV[b]
1a	0.62 (1e⁻), 0.75 (1e⁻), 0.84 (4e⁻)	130	120[c]
1b	1.11 (6e⁻)	0	—[d]
1c	0.51 (1e⁻), 0.64 (1e⁻), 0.74 (1e⁻), 0.86 (3e⁻)	130	230
1d	0.57 (1e⁻), 0.69 (1e⁻), 0.77 (1e⁻), 0.86 (3e⁻)	120	170[c]
2	0.94 (2e⁻), 1.11 (1e⁻), 1.34 (1e⁻), 1.46 (1e⁻), 1.59 (1e⁻)	0	—[d]
3	∼ 1.3 (irrev)	—	—[d]
4	0.74 (1e⁻)	0	0
5	0.63 (1e⁻), 0.82 (1e⁻)	190	110
6	0.67 (1e⁻), 0.77 (1e⁻), 0.87 (3e⁻)	100	70

[a] Potential difference between the first and second anodic waves. [b] Difference between the potential of the first oxidation wave and that of the mononuclear donor. [c] Relative to *N*-Me,Et-substituted mononuclear donor. [d] Mononuclear analogue unavailable.

Charts 4−6 was first examined by transient electrochemical techniques since their distinctive anodic behaviors were strongly dependent on the number as well as the type of redox center. For example, the initial positive-scan cyclic voltammogram (CV) of parent donor **4**, containing only a single anilinyl redox center, showed a reversible one-electron (1e⁻) oxidation wave at 0.74 V vs SCE (Figure 2a), which is essentially that of *N,N*-diethyltoluidine itself, with $E_{1/2}$ = 0.76 V. By comparison, the dinuclear *ortho*-dianilinyl dyad **5** showed reversible anodic waves at $E_{1/2}$ = 0.63 and 0.82 V (Figure 2b), with each wave corresponding to a 1e⁻ process. Such a pair of oxidation waves is well known for different types of mixed-valence systems,[8,9,29] and the magnitude of the splitting (ΔE, as listed in Table 1, second column) is directly related to the degree of electronic interaction between the oxidized and neutral donor centers in Chart 1.[30]

The pentaanilinyl and hexaanilinyl donors **6** and **1c,d** showed further splittings of the oxidation waves. Thus, the cyclic voltammogram of **1c** revealed four reversible anodic waves at 0.51, 0.64, 0.74, and 0.86 V; controlled-potential coulometry (see Experimental Section) indicated the first, second, and third waves to correspond to 1e⁻ processes and the fourth wave to an unresolved 3e⁻ process (Table 1). The peak potential and relative (peak-current) intensity of the oxidation waves for this polynuclear donor were confirmed by Osteryoung square-wave voltammetry (OSWV), as shown in Figure 2d. As such, the initial production of the p-doped cation-radical **1c**•⁺ at $E_{1/2}$ =

0.51 V was clearly separated from its subsequent oxidation at $E_{1/2}$ = 0.64 V to the dication and thence to the trication at $E_{1/2}$ = 0.74 V; the fourth anodic wave corresponded to an overall 3e⁻ process at $E_{1/2}$ = 0.86V (eq 1). Essentially the same CV

$$\mathbf{1c} \underset{(0.51\ \mathrm{V})}{\overset{1e^-}{\rightleftharpoons}} \mathbf{1c}^{\bullet+} \underset{(0.64\ \mathrm{V})}{\overset{1e^-}{\rightleftharpoons}} \mathbf{1c}^{2+} \underset{(0.74\ \mathrm{V})}{\overset{1e^-}{\rightleftharpoons}} \mathbf{1c}^{\bullet3+} \underset{(0.86\ \mathrm{V})}{\overset{3e^-}{\rightleftharpoons}} \mathbf{1c}^{6+} \tag{1}$$

behavior was found for donor **1d** (Table 1). Furthermore, the CV and OSWV behaviors of the hexapiperidinyl donor (**1a**) were similar in shape to those of **1c** and **1d**, but incompletely resolved (see Supporting Information, Figure S1), and their computer simulation indicated that the first and second waves corresponded to 1e⁻ processes and the third wave to an overall 4e⁻ process (see the relevant oxidation potentials in Table 1).

CV and OSWV measurements of the pentaanilinyl donor **6** revealed two reversible waves at 0.67 and 0.77 V and a broad reversible (composite) wave at 0.87 V vs SCE (Figure 1C). Computer simulation indicated an approximately 1:1:3 intensity ratio, which suggested that these corresponded to successive 1e⁻/1e⁻/3e⁻ processes.

In comparison to the voltammetric behavior of the dialkyl-anilinyl donors **1a**, **1c**, and **1d**, showing significant splittings of their oxidation waves, the cyclic voltammogram of the bis-(*p*-bromophenyl)amino derivative **1b** revealed only a single reversible anodic wave at $E_{1/2}$ = 1.11 V, corresponding to an unresolved 6e⁻ process (Figure S1B).[31] This oxidation potential coincided with $E_{1/2}$ = 1.11 V for the reversible 1e⁻ oxidation of tris(*p*-bromophenyl)amine to the corresponding cation-radical. The hexacarbazole donor **2** showed four reversible oxidation waves at $E_{1/2}$ = 0.94, 1.11, 1.34, and 1.46 V, in which the first wave corresponded to an unresolved 2e⁻ process and each of the other three waves corresponded to 1e⁻ processes (Figure S1C). The fifth *irreversible* wave for the final 1e⁻ process, to afford the hexacation, was observed in the OSW voltammogram at $E_{1/2}$ = 1.59 V.[32] Finally, the hexapyrrole donor **3** showed only unresolved irreversible oxidation waves in its voltammograms.

Most importantly, the first anodic wave of each of the five *N,N*-dialkyl-substituted anilinyl donors in Table 1, that corresponded to the production of the p-doped cation-radicals **1a**•⁺, **1c**•⁺, **1d**•⁺, **5**•⁺, and **6**•⁺, all occurred at potentials significantly negative-shifted by an amount δE relative to that of the *N,N*-

(29) (a) Lahlil, K.; Moradpour, A.; Bowlas, C.; Menou, F.; Cassoux, P.; Bonvoisin, J.; Launay, J.-P.; Dive, G.; Dehareng, D. *J. Am. Chem. Soc.* **1995**, *117*, 9995. (b) Nelsen, S. F.; Ismagilov, R. F.; Powell, D. R. *J. Am. Chem. Soc.* **1997**, *119*, 10213. (c) Lindeman, S. V.; Rosokha, S. V.; Sun, D.-L.; Kochi, J. K. *J. Am. Chem. Soc.* **2002**, *124*, 843. (d) Risko, C.; Barlow, S.; Coropceanu, V.; Halik, M.; Brédas, J.-L.; Marder, S. R. *Chem. Commun.* **2003**, 194.
(30) Evans, C. E. B.; Naklicki, M. L.; Rezvani, A. R.; White, C. A.; Kondratiev, V. V.; Crutchley, R. J. *J. Am. Chem. Soc.* **1998**, *120*, 13096.

(31) A similar single broad oxidation wave (simulated as six 1e⁻ waves with close potentials) was previously obtained for hexakis[4-(*N,N*-(dimethoxy-phenyl)amino)phenyl]benzene.[18b]
(32) (a) The related 1,2,4,5-tetracarbazolyl-3,6-difluorobenzene shows three oxidation waves at $E_{1/2}$ = 1.08 (2e⁻), 1.23 (1e⁻), and 1.38 V (1e⁻) vs SCE (Figure S1D). (b) Note that the cyclic voltammogram of the hexakiscarbazolylbenzene donor **2** in Figure S1C was arbitrary truncated at 1.5 V because the oxidation to the hexacation was chemically irreversible. By comparison, square-wave voltammetry does not limit the potential sweep.

dialkylaniline, as listed in the last column of Table 1. These electrochemical studies also indicated that only the polyanilinyl donors **1c**, **1d**, **4**, **5**, and **6** showed cleanly separated first oxidation states; this unique voltammetric feature allowed us to isolate and characterize the corresponding p-doped mono-cations and identify the comparative effects of varying numbers and types of redox centers on the p-doping properties, as follows.

III. Isolation of p-Doped Hexaarylbenzene Cation-Radical Salts. Although the facile generation of the p-doped hexaaryl-benzenes listed in Table 1 revealed their persistent character, the various electrochemical methodologies were not readily applicable to the isolation of the cation-radical salts owing to the experimental difficulties in effectively separating the supporting electrolytes. To circumvent the latter, we identified the dodecamethylcarboranyl radical **CB•** as the viable *uncharged* oxidant[33] owing to its oxidation potential of $E_{ox}° = 1.41$ V vs SCE, together with its blue color ($\lambda_{max} = 905$ nm, $\epsilon = 550$ M^{-1} cm^{-1}) in dichloromethane solutions. As such, the p-doped cation-radicals **4•+** and **5•+** of the mono- and dinuclear donors were readily prepared in the one-electron oxidation of the corresponding neutral donors in dichloromethane at -28 °C with a stoichiometric (1:1) amount of **CB•**. The paramagnetic salts **4•+ CB⁻** and **5•+ CB⁻** were separated in nearly quantitative yield simply by addition of hexane, and their purity was found by spectral titration to be >98% (see Experimental Section). In a similar manner, the desirable p-doped hexanuclear cation-radical salts **1c•+ CB⁻** and **1d•+ CB⁻** were also isolated as dark blue powders in essentially quantitative yields with high (>96%) purity, i.e.

$$(2)$$
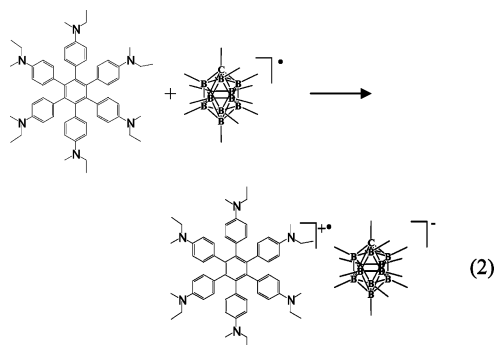
Reduction of the blue solid with zinc dust in dichloromethane solution led to the quantitative recovery of more than 96% of the neutral hexaarylbenzene donor (**1c**).

Moreover, treatment of the pentanuclear donor **6** (containing a triflate counterion) with 1 equiv of carboranyl radical led to a similar 1e⁻ oxidation, to yield the p-doped dication-radical **6•+**, the complex mixed (OTf⁻)(CB⁻) salt of which was not isolated in solid form (vide infra).

It is important to emphasize that the significant difference between the first and second oxidation potentials of the pertinent donors — **1c**, **1d**, and **4**−**6** — excluded the disproportionation of these p-doped cation-radicals into the corresponding neutral donor and the dication as a complicating factor since the disproportionation (equilibrium) constants based on $\ln K_D = F\Delta E$ were predicted to be $K_D < 10^{-2}$ for $\Delta E > 100$ mV in Table 1. Nonetheless, the unavoidable admixture of small
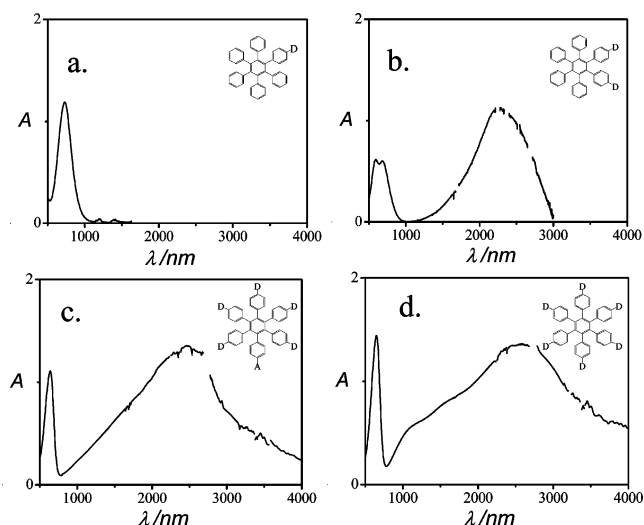
(33) For the preparation and characterization of **CB•**, see: King, B. T.; Noll, B. C.; McKinley, A. J.; Michl, J. *J. Am. Chem. Soc.* **1996**, *118*, 10902.

Figure 3. Electronic spectra of the p-doped mononuclear **4•+** (a), dinuclear **5•+** (b), pentanuclear **6•+** (c), and hexanuclear **1c•+** (d) cation-radicals, with D = Et₂N and A = MeEt₂N⁺ substituents.

Table 2. Electronic Spectral Data for p-Doped Polyanilinylbenzenes

cation-radicals	λ_{max}, nm (ϵ_{max}, cm^{-1} M^{-1})
1a•+	657 (3700), 1000−3300 (br)
1c•+	657 (3900), 2570 (br, 3300)
1d•+	656 (3900), 2570 (br)
4•+	732 (3000)
5•+	596 (1600), 683 (1600), 2300 (2800)
6•+	650 (3500), 2400 (3000)

amounts of multiply charged cations inhibited the clean growth of single crystals of **1c•+**, **1d•+**, and **5•+** suitable for X-ray analysis, despite our various attempts at recrystallization.

IV. Spectroscopic Characterizations of p-Doped Hexaaryl-benzene Cation-Radicals. A. Electronic and ESR Spectra of Mono- and Dinuclear Cation-Radicals 4•+ and 5•+. The electronic spectrum (Figure 3a) of the mononuclear cation-radical **4•+** in dichloromethane solution consisted of only a single absorption band at $\lambda_{max} \approx 732$ nm, which was readily assigned to the local transition in the redox center.[34] The temperature-independent ESR spectrum of **4•+** was characterized by partially resolved hyperfine splittings arising from one nitrogen and hydrogens of the alkyl substituents and benzene ring (Figure S2).

In strong contrast, the electronic spectrum of the dinuclear cation-radical **5•+** showed twin absorption bands in the visible region ($\lambda_{max} = 596$ and 683 nm, Table 2). More importantly, this dinuclear cation-radical exhibited a new strong absorption band (Figure 3b) in the near-IR region, with $\lambda_{max} = 2300$ nm, which was absent in the mononuclear analogue **4•+** (Table 2). As such, this NIR band was assigned to the intervalence transition (characteristic of mixed-valence compounds)[6,8,9,35] resulting from interaction of the oxidized and the neutral redox centers. The ESR spectrum of the dinuclear cation-radical **5•+** consisted of a single (unresolved) broad band at all temperatures and concentrations studied.

(34) Shida, T.; Nosaka, Y.; Kato, T. *J. Phys. Chem.* **1978**, *82*, 695.
(35) (a) Coropceanu, V.; Malagoli, M.; Andre, J. M.; Brédas, J. L. *J. Am. Chem. Soc.* **2002**, *124*, 10519. (b) Barlow, S.; Risko, C.; Chung, S.-J.; Tucker, N. M.; Coropceanu, V.; Jones, S. C.; Levi, Z.; Bredas, J.-L.; Marder, S. R. *J. Am. Chem. Soc.* **2005**, *127*, 16900.
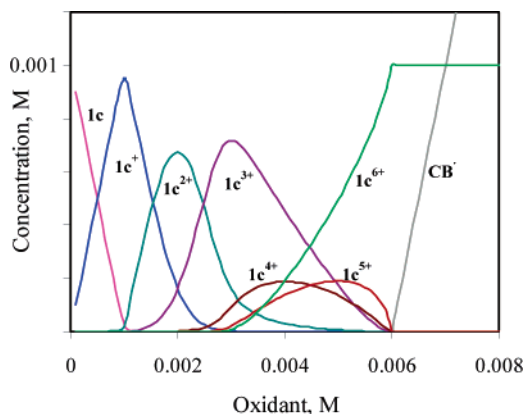
Figure 4. Equilibrium concentrations of the different oxidation states formed upon the incremental addition of **CB•** to a 1 mM solution of donor **1c**.
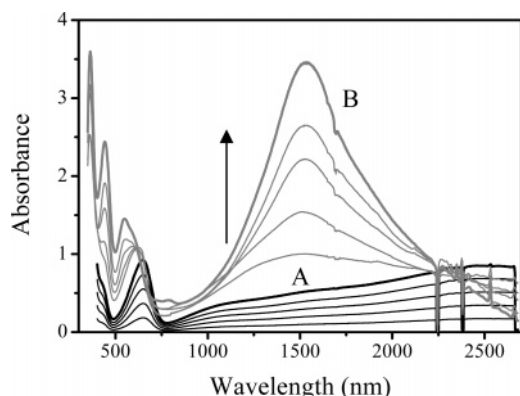

Figure 5. Typical spectral changes upon the addition (in 0.2 M increments) of oxidant to a 1 mM solution of hexanuclear donor **1d**, showing the rise of spectrum A (black lines) in 0:1 to 1:1 oxidant-to-donor ratios and its transformation to spectrum B (gray lines) with further additions of oxidant.

B. Electronic and ESR Spectra of p-Doped Hexaarylbenzene Cation-Radicals. Owing to the multiple oxidation states that are readily available to the hexaarylbenzene donors listed in Table 1, it was necessary to carefully deconvolute the spectral changes accompanying p-doping into the component spectra of the mono-, di-, tri-, etc. cationic species. For example, as a result of the presence of six redox centers, the oxidation of hexanuclear donor **1c** led to a complex set of equilibria among seven oxidation states (from 0 to 6+), the relative concentrations of which were established by the differences in the redox potentials according to the Nernstian relationship. As such, the values of the oxidation potentials in Table 1 allowed us to calculate the equilibrium concentrations of the different oxidation states when **CB•** was incrementally added to the donor; the quantitative computer simulation (see Experimental Section for details) of the redox equilibria leading to typical equilibrium dependences of the different oxidation states is presented in Figure 4.

To quantitatively ascertain the spectral properties of the p-doped hexaarylbenzene (**1c•+** and higher oxidation states), we first carried out the spectrochemical titration by the stepwise addition of the strong (uncharged) oxidant **CB•** to a solution of the hexaanilinylbenzene in dichloromethane under conditions in which the 1 mM solution of neutral donor **1d** showed no absorption in the vis−NIR region (Figure 5). First, the addition of a small amount (0.2 mM) of **CB•** immediately led to the appearance of a new sharp band at $\lambda_{max} = 657$ nm, together with a broad absorption in the 1000−3000 nm range (Figure

5). Further incremental additions of oxidant were accompanied by the rise in intensity of these absorptions, but their shapes (hereinafter referred to as spectrum A) remained essentially unchanged until the concentration of **CB•** became equal to the concentration of the donor. As more oxidant was added (from 1:1 to 2:1 equiv), the shape of the spectrum changed, and the intensity of another absorption at 1530 nm grew significantly, whereas the absorption at 2570 nm decreased with the concomitant appearance of an isosbestic point at 2300 nm. The intensity of the 657-nm band decreased, and new bands appeared at 545 and 450 nm.[36] As a result, a new intense absorption band (spectrum B) with narrow bandwidth was apparent at $\lambda_{max} = 1530$ nm and optimized at the oxidant/donor ratio of 2:1. Further increases in oxidant concentration led to an intensity decrease since the multiply charged cations (3+ to 6+) did not show clear absorption in the NIR region (see Figure S3 in the Supporting Information).

Quantitative spectral comparison at different oxidant/donor ratios with the corresponding concentrations of the different oxidation states in Figure 5 indicated that spectra A and B were directly related to the monocation (**1d•+**) and the dication (**1d²⁺**), respectively. In particular, the experimental spectra measured in the titration window between the 0:1 and 2:1 ratios of oxidant to donor were well simulated as the simple superposition of the individual spectra of monocation and dication with each multiplied by its relative concentration taken from Figure 4.[36] This procedure allowed the unambiguous assignment of the spectrum A (recorded at 1:1 oxidant/donor ratio in Figure 5, bold curve) to **1d•+**. The highly distinctive (and unprecedented) electronic transitions extant in this monocation are underscored by the exceptionally broad low-energy intervalence envelope (containing partially resolved components) that stretches continuously from the visible (red) region all the way down to the infrared region beyond 4000 nm (with a nominal maximum at $\lambda_{max} = 2570$ nm, $\epsilon = 3300$ M^{-1} cm^{-1}) — certainly by comparison to the simple near-Gaussian band of the dyad analogue **5•+** in Figure 3b.[37] Moreover, the oxidative titration of the hexanuclear donor **1c** also led to essentially the same spectral changes, and the complete (UV−NIR) spectrum of the p-doped monocation **1c•+** is shown in Figure 3d.[38] Most importantly, the dissolution of the dark blue powder isolated as the **1c•+ CB⁻** salt in eq 2 produced the same electronic spectrum as that obtained by the spectrochemical titration at the 1:1 oxidant/donor ratio. The ESR spectrum of **1c•+** showed only one broad, unresolved peak at $g = 2.0026$ in the temperature range from +20 to −88 °C.

C. Spectral Characterization of the p-Doped Pentanuclear Dication-Radical 6•+. The calculated distributions of the various

(36) As the oxidant/donor ratio approached 2:1, the spectra deviated from this isosbestic point due to intrusion of the trication **1c³⁺** (Figure 5); thus, the spectra could not be reliably simulated as the linear superposition of the mono- and dication spectra.

(37) The abrupt drop (cutoff) of the low-energy half of the intervalence absorption of **5•+** (under conditions in which the high-energy half is Gaussian, as shown in Figure S10) also indicates that the value of H_{ab} is significant as compared to $\lambda/2$.[9] Such a mixed-valence cation-radical at the Class II/III border has been appropriately described by Nelsen as "almost delocalized".[9b]

(38) (a) Addition of an excess of the neutral donor **1c** to the solution containing a 1:1 donor/oxidant ratio did not materially change the electronic spectrum in the vis−NIR range, and this supports its assignment to the cation-radical **1c•+**. (b) To compensate the molecular vibration components, the solution of the neutral donor at the same concentration was used as the reference for baseline measurements in the region $\lambda = 3000-4000$ nm (see Figure S9 in the Supporting Information).

oxidation states in the solution of the pentanuclear donor **6** upon successive additions of the carborane radical in the 0:2 oxidant-to-donor ratios were similar to those of the hexaanilinylbenzenes **1c** and **1d** (since the differences between the first, second, and third oxidation waves were roughly the same in both systems). In fact, the addition of small amounts of the carborane radical to the solution of **6** led to the appearance of the band at 650 nm, corresponding to the local absorption of the pentaanilinyl cation-radical, together with its broad intervalence band with maximum around 2400 nm in the NIR region. The intensities of both of these bands increased more or less linearly until the oxidant/donor ratio attained 1:1. Further additions of carborane radical led to the decrease in the intensity of the low-energy half of the NIR band, an increase of the absorption around 1050 nm, and a shift of the absorption band at 650 nm. As a result, at the 2:1 oxidant/donor ratio, quite a different spectrum was observed, with maxima at 558 and 1050 nm (Figure S4). As such, the NIR spectrum at oxidant/donor ratios less than or equal to 1:1 can be readily assigned to that of the cation-radical, as shown in Figure 3c alongside the cation-radical spectra of other aniline-substituted benzenes. ESR measurements revealed that the cation-radical $6^{\bullet+}$ was characterized by a broad, unresolved signal similar to that of either $1c^{\bullet+}$ or $1d^{\bullet+}$.

Discussion

The characteristic but highly unusual redox behaviors of the hexanuclear donors in Figure 2 lead to the distinctive hexanuclear cation-radicals $1c^{\bullet+}$ and $1d^{\bullet+}$, showing unique electronic absorption bands stretching continuously from the visible (red) to well beyond 4000 nm in the infrared spectral region, and clearly consisting of multiple (partially) resolved components. Such a complex intervalence transition in the p-doped hexanuclear donors $1c^{\bullet+}$ and $1d^{\bullet+}$ (Figure 3d) strongly contrasts with the more usual intervalence band shown by a dinuclear analogue such as $5^{\bullet+}$, in which the electronic transition (see Figure 3b) relates to a single Gaussian envelope truncated at the low-energy edge (Figure S10) in a manner that was previously characterized for Robin–Day Class II mixed-valence systems at or near the Class III border.[9] As such, let us first consider whether the p-doped dinuclear cation-radical $5^{\bullet+}$ can be theoretically treated as such a mixed-valence system and the electron movements within the p-doped stacked array assessed in a quantitative manner by the application of Marcus electron-transfer theory.[6,11,39] The simplest aromatic array consisting of the p-doped dyad depicted in Chart 1 is to be considered the *self-exchange* between bridged Ar/Ar$^{\bullet+}$ redox centers; within the context of the later Marcus–Sutin development,[40] the rate of such an electron movement is governed by the reorganization energy λ and the coupling element H_{ab}, so the activation energy for the dynamic electron-transfer process is

$$\Delta G_{ET}^* = (\lambda - 2H_{ab})^2/4\lambda \qquad (3)$$

I. Evaluation of the Reorganization Energy and Electronic Coupling Element for the p-Doped Dinuclear Dyad ($5^{\bullet+}$).

The critical values of H_{ab} for strongly coupled dyads such as

those included in Chart 1 are identified experimentally by their unique optical transitions (usually occurring in the near-IR region) that Hush[41] characterized as the intervalence absorption bands (ν_{IV}) on the basis of the earlier Mulliken charge-transfer formulation for organic donor/acceptor systems.[42] According to the Mulliken–Hush two-state analysis,[43] the adiabatic ground- and excited-state wave functions (Ψ_1 and Ψ_2) of the p-doped dinuclear donor ($5^{\bullet+}$) are expressed via the diabatic initial and final states (ψ_a and ψ_b) as $\Psi_1 = a\psi_a + b\psi_b$ and $\Psi_2 = b\psi_b - a\psi_a$. The solution of the corresponding secular 2×2 determinant leads to the energies of adiabatic states (E_1, E_2) and optical transition (ν_{IV}), expressed as[44]

$$E_{2,1} = \frac{H_{aa} + H_{bb}}{2} \pm \frac{((H_{bb} - H_{aa})^2 + 4H_{ab}{}^2)^{1/2}}{2} \qquad (4)$$

$$\nu_{IV} = E_2 - E_1 = ((H_{bb} - H_{aa})^2 + 4H_{ab}{}^2)^{1/2} \qquad (5)$$

where H_{aa} and H_{bb} are the energies of the initial and final states and $H_{ab} = \int \psi_a H \psi_b$ is the electronic coupling element. For "localized" Robin–Day Class II mixed-valence systems[10] (which are characterized by relatively small values of the electronic coupling with $0 < H_{ab} < \lambda/2$), the maximum of the intervalence transition (ν_{IV}) corresponds to the reorganization energy, i.e., $\lambda = \nu_{IV}$. The coupling element H_{ab} is evaluated experimentally via the Mulliken–Hush formalism:[45]

$$H_{ab}{}^{MH} = \frac{0.0206(\nu_{IV} \int \epsilon(\nu) \, d\nu)^{1/2}}{r_{DA}} \qquad (6)$$

where $\int \epsilon(\nu) \, d\nu$ is the integrated intensity (oscillator strength) of the intervalence absorption band and r_{ab} is the separation (Å) between the redox centers.[46] Application of eq 6 to the intervalence absorption of cation-radical $5^{\bullet+}$ (with $\nu_{IV} = 4.35 \times 10^3$ cm^{-1} and $\int \epsilon(\nu) \, d\nu = 5.52 \times 10^6$), together with $r_{DA} = 7.0$ Å (taken as the distance between the nitrogen centers), leads to $H_{ab}{}^{MH} = 460$ cm^{-1}, which is much less than $\lambda = 4350$ cm^{-1}, in agreement with the assignment of $5^{\bullet+}$ as a Robin–Day Class II mixed-valence monocation.

(41) Hush, N. S. *Prog. Inorg. Chem.* **1967**, *8*, 391.

(42) (a) Mulliken, R. S.; Person, W. B. *Molecular Complexes*; Wiley: New York, 1969. (b) It is important to emphasize that Hush *intervalence* transitions are a special case of the more general Mulliken *charge-transfer* transitions.[10a,35] Furthermore, the *charge-resonance* transition also represents a special case of charge-transfer transitions.[3h] All three phenomena relate to intermolecular optical transitions associated with the electronic interaction between the HOMO of an electron-rich donor and the LUMO of an electron-poor acceptor.

(43) (a) Creutz, C.; Newton, M. D.; Sutin, N. *J. Photochem. Photobiol. A: Chem.* **1994**, *82*, 47. (b) Brunschwig, B. S.; Sutin, N. In *Electron Transfer in Chemistry, Vol. 2*; Balzani, V., Ed.; Wiley: New York, 2001; p 583.

(44) For $5^{\bullet+}$, the diabatic states represent hypothetical non-interacting states with the hole localized on one redox center. The energies of the diabatic states show quadratic dependence on the reaction coordinate with minima located at $X = 0$ and 1; i.e., $H_{aa} = \lambda X^2$ and $H_{bb} = \lambda(X - 1)^2$,[40] see Figure 6.

(45) Significant deviation of the intervalence band of $5^{\bullet+}$ from a Gaussian shape[37] (Figure S10) prevented the use of the common expression based on $H_{ab}{}^{MH} = 0.0206(\nu_{IV} \Delta\nu\epsilon)^{1/2}/r_{DA}$.

(46) (a) The application of eq 6 often suffers from difficulties associated with the proper choice of r_{ab}, especially for organic species with significant charge delocalization.[6,9,29] (b) Nelsen, S. F.; Newton, M. D. *J. Phys. Chem. A* **2000**, *104*, 10023. (c) Coropceanu, V.; Gruhn, N. E.; Barlow, S.; Lambert, C.; Durivage, J. C.; Bill, T. G.; Noell, G.; Marder, S. R.; Bredas, J.-L. *J. Am. Chem. Soc.* **2004**, *126*, 2727. (d) In addition, as pointed out by a reviewer, charge delocalization over the phenyl groups with center-to-center separation of 4.3 Å results in significant shortening of the effective charge-transfer distance r_{ab} and a corresponding increase of the calculated coupling element.

(39) For recent reviews, see: (a) Newton M. D. *Electron Transfer in Chemistry, Vol. 1*; Balzani, V., Ed.; Wiley-VCH: New York, 2001; p 3. (b) Newton, M. D. *Coord. Chem. Rev.* **2003**, *238–239*, 167.

(40) (a) Brunschwig, B. S.; Sutin, N. *Coord. Chem. Rev.* **1999**, *187*, 233. (b) Sutin, N. *Adv. Chem. Phys.* **1999**, *106*, 7.

Importantly, the electronic interaction between redox sites results in the stabilization of the Ar/Ar$^{\bullet+}$ dyad relative to the isolated Ar and Ar$^{\bullet+}$ centers, and the free energy of stabilization is related to the electronic coupling and the reorganization energy as $\Delta G_r = -H_{ab}^2/\lambda$.[30,40] Such a stabilization is the major factor determining the splittings in the electrochemical oxidation of **5** into two waves in Figure 1b, so $\Delta E \approx 2\Delta G_r/F$.[40] Accordingly, the value of the electronic coupling element can be estimated from the electrochemical data, and the splitting of $\Delta E = 190$ mV in Table 1 leads to $H_{ab}^{CV} = 1800$ cm^{-1}. This estimate confirms the assignment of **5**$^{\bullet+}$ to Class II, but the magnitude of H_{ab}^{CV} is significantly higher than that estimated from the spectral data (H_{ab}^{MH}). To reconcile this discrepancy, let us consider both methods more critically.

On one hand, the splitting of the oxidation waves of the Ar/Ar$^{\bullet+}$ dyad is affected not only by resonance stabilization but also by some additional entropy, electrostatic, and other factors.[30] Therefore, the CV-based value represents an upper limit of the electronic coupling (i.e., $H_{ab} < H_{ab}^{CV}$). On the other hand, recent studies show that the proper separation parameter r_{ab} in eq 8, in many cases, is only 50–60% of the value determined from the molecular geometry.[46] Since any decrease of r_{ab} increases H_{ab}^{MH}, the value calculated with $r_{ab} = 7$ Å should be considered as a lower limit of electronic coupling element (i.e., $H_{ab} > H_{ab}^{MH}$). We thus conclude that the spectral and electrochemical data provide upper and lower limits for the electronic coupling element, and the optical and thermal electron transfer in the dinuclear cation-radical **5**$^{\bullet+}$ can be consistently described within the framework of the two-state analysis using the reorganization energy, $\lambda \approx 4400$ cm^{-1}, and the electronic coupling, $H_{ab} \approx 1000–1700$ cm^{-1}.[37]

The extent to which the value of H_{ab} approaches the reorganization energy, the activation barrier for electron movement, is significantly lowered so that, within the p-doped Ar/Ar$^{\bullet+}$ dyad with $\lambda \approx 4400$ cm^{-1} and $H_{ab} \approx 1300$ cm^{-1}, the value of ΔG_{ET}^* according to eq 5 is only ~0.5 kcal mol^{-1}, relative to the barrier of 3.1 kcal mol^{-1} in the absence of electronic coupling, as illustrated in Figure 6.

II. Electron Delocalization in p-Doped Hexanuclear Donors. Owing to the presence of six equivalent redox centers, the adiabatic ground-state and excited-state wave functions (Ψ_1, ..., Ψ_6) of the p-doped hexanuclear donors (**1c**$^{\bullet+}$ and **1d**$^{\bullet+}$) are expressed via six diabatic initial and final states, ψ_a, ..., ψ_f:

$$\Psi_1 = a_1\psi_a + b_1\psi_b + c_1\psi_c + d_1\psi_d + e_1\psi_e + f_1\psi_f \quad (7a)$$

$$\vdots$$

$$\Psi_6 = a_6\psi_a + b_6\psi_b + c_6\psi_c + d_6\psi_d + e_6\psi_e + f_6\psi_f \quad (7f)$$

[For the visualization of the noninteracting (diabatic) states with the hole localized on different redox centers, see Chart S1 in the Supporting Information.] To simplify the secular 6×6 determinant, we explicitly take into account only interactions (H_{ab}) between neighboring anilinyl groups (neglecting the expectedly weak interactions between meta and para substituents).[18b] Furthermore, we assign the zero points of the reaction coordinate and the energy to the diabatic state with the electron on the redox center "a" and relaxed nuclear geometries for all six centers[47a] (i.e., $H_{aa} = 0$ at $X = 0$). Under such conditions, the energies of all other diabatic states at the same point of the
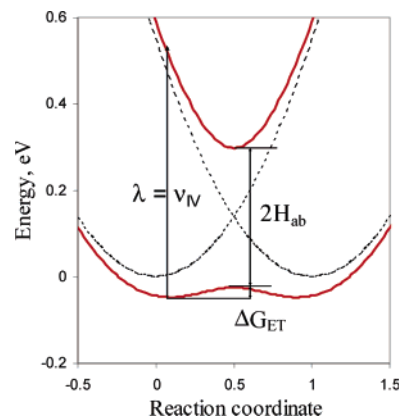

Figure 6. Energy diagrams for electron transfer within the p-doped dinuclear donor with the diabatic reactant and product states of **5**$^{\bullet+}$ shown as dashed lines, and the adiabatic ground state and excited state shown as red (solid) lines.

nuclear reaction coordinate (Franck–Condon excitation) are equal to the reorganization energy, λ.[47b] The solution of the corresponding secular determinant (Chart S3) with the aid of the Mathematica 4.1 program[48] yields the exact eigenenergies (E_i) as a complex function of H_{ab} and λ (Chart S4). However, for illustrative purposes, Table 3 shows semiquantitatively how the eigenenergies vary as a function of H_{ab} and λ by arbitrarily truncating the exact solution at second order — likewise for the coefficients of the adiabatic wave functions at third order.[49] The latter reflect the relative odd-electron population on each redox site, and Chart 7 qualitatively depicts the relative electron population on each redox site for the adiabatic wave functions Ψ_1, ..., Ψ_6.

The results in Table 3 thus predict that the intervalence absorption of hexanuclear cation-radicals **1**$^{\bullet+}$ potentially[50]

(47) (a) That is, the geometry at the center "a" corresponds to that of the cationic center and all others to the neutral anilinyl group. (b) Indeed, the terms H_{aa}, ..., H_{ff} refer to the energies of diabatic (non-interacting) states ψ_a, ..., ψ_f, which correspond to six isolated non-interacting redox sites with the hole localized on the sites a–f, respectively, as illustrated in Chart S1 in the Supporting Information. Furthermore, the diabatic state ψ_a, with relaxed nuclear geometry of all six centers (i.e., relaxed geometry of cationic center a and relaxed geometries of neutral centers b–f), was set as the zero point of the reaction coordinate, i.e., at $X = 0$, $H_{aa} = E_{aC} + E_{bN} + E_{cN} + E_{dN} + E_{eN} + E_{fN} = 0$, where E_{aC} represents the energy of the cationic center in the relaxed geometry and E_{bN}, ..., E_{fN} are the energies of the neutral centers in the relaxed geometries. At the same point of $X = 0$, the nuclear geometries of diabatic states ψ_b, ..., ψ_f are the same as the relaxed geometry of state ψ_a, but the hole is transferred from site a to one of the sites b–f, respectively. Thus, at $X = 0$, the energy of the diabatic state ψ_b is $H_{bb} = E_{aN}^* + E_{bC}^* + E_{cN} + E_{dN} + E_{eN} + E_{fN}$, where E_{aN}^* is the energy of the neutral center a with the nuclear geometry of the (relaxed) cation and E_{bC}^* is the energy of the cationic center b with the geometry of the neutral center. Since all the redox centers are equivalent and they do not interact in the diabatic states, the notation a–f can be omitted, and the expression can be rewritten as $H_{bb} = E_N^* + E_C^* + 4E_N$. Addition and subtraction of the term $E_C + E_N$ leads to $H_{bb} = (E_N^* + E_C^* - E_C - E_N) + (E_C + 5E_N)$. The term in the first set of parentheses represents the reorganization energy, λ, and the term in the second set of parentheses is $H_{aa} = 0$. Therefore, it follows that $H_{bb} = \lambda$. Furthermore, if the relaxed nuclear geometry of the diabatic state ψ_a is frozen and the hole is transferred to one of the (non-interacting) sites c–f, the same procedure results in $H_{cc} = H_{dd} = H_{ee} = H_{ff} = \lambda$.

(48) *Mathematica*, Version 4.1; Wolfram Research, Inc.: Champaign, IL 61820-7237.

(49) In Table 3, the higher-order H_{ab}/λ terms were neglected. However, the numerical values of eigenenergies E_i and coefficients a_i–f_i listed in Table S1 were obtained by the exact solution of the 6×6 determinant in Chart S3 with $H_{ab} = 1900$ cm^{-1} and $\lambda = 5500$ cm^{-1} via Mathematica 4.1 using the N[Eigenvalues[...]] and N[Eigenvectors[...]] options;[48] these E_i and a_i–f_i values were used for the calculation of transition energies ν_i^{THEO} and their relative intensities for the hexad **1c**$^{\bullet+}$ in Table 4. In a similar way, the exact solution of the 5×5 determinant in Chart S5 produces the values of E_i and a_i–e_i listed in Table S2, which lead to the transition energies ν_i^{THEO} and their relative intensities for the pentad **6**$^{\bullet+}$ in Table 6.

(50) Some of the transitions could be symmetry-forbidden, vide infra.

Table 3. Energies (E_i) and Coefficients (a_i–f_i) of the Adiabatic States, Approximated in Terms of the Reorganization Energy λ and Coupling Element H_{ab}[49]

		coefficients[a]					
i	energy	a	b	c	d	e	f
1	$-H_{ab}^2/\lambda$	1	H_{ab}/λ	H_{ab}^2/λ^2	$2H_{ab}^3/\lambda^3$	H_{ab}^2/λ^2	H_{ab}/λ
2	$\lambda - H_{ab}\sqrt{3} + H_{ab}^2/3\lambda$	$2H_{ab}/\lambda$	-1	$-\sqrt{3}$	-2	$-\sqrt{3}$	-1
3	$\lambda - H_{ab}$	0	-1	-1	0	1	1
4	$\lambda + 4H_{ab}^2/3\lambda$	$2H_{ab}/\lambda$	-1	$-2H_{ab}/3\lambda$	1	$-2H_{ab}/3\lambda$	-1
5	$\lambda + H_{ab}$	0	1	-1	0	1	-1
6	$\lambda + H_{ab}\sqrt{3} + H_{ab}^2/\lambda$	$2H_{ab}/\lambda$	-1	$\sqrt{3}$	-2	$\sqrt{3}$	-1

[a] For simplicity of representation, the eigenvectors are not normalized.

Chart 7
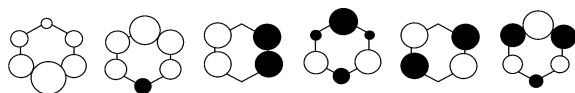
contains five optical transitions with energies $\nu_i = E_{(i+1)} - E_1$, where $i = 1$–5, in sharp contrast to the dinuclear cation-radical **5•+**, which is characterized by a single electronic transition ($\nu_{IV} = \lambda$). Notably, all optical transitions are characterized by essentially the same energy ($\nu \approx \lambda$) if the coupling element is small ($H_{ab} \ll \lambda$). However, any significant coupling between redox sites leads to the noticeable separation of electronic transitions (e.g., the energy difference between the highest and lowest transitions is $\nu_5 - \nu_1 \approx 2H_{ab}\sqrt{3}$). This results in the considerable broadening of the intervalence spectrum and its ultimate resolution into individual (electronic) components. Indeed, the experimental electronic spectrum of the hexanuclear cation-radical **1c•+** in Figure 3d shows quite a broad intervalence NIR absorption band (containing several components) and indicates that significant coupling occurs between multiple redox centers.[51]

To experimentally evaluate λ and H_{ab} from the intervalence absorption, the coupling element is first estimated as $H_{ab} = 1590$ cm^{-1} from the difference between the low-energy maximum (~3500 cm^{-1}) and the high-energy half (~9000 cm^{-1}), given as $\nu_5 - \nu_1 \approx 2H_{ab}\sqrt{3}$. Next, the reorganization energy is estimated as $\lambda = 5500$ cm^{-1} from the lowest-energy maximum, given as $\nu_1 = E_2 - E_1 \approx \lambda - H_{ab}\sqrt{3} + 2H_{ab}^2/\lambda$, as listed in Table 3. The solution of the determinant in Chart S3 with these values of H_{ab} and λ leads to the transition energies ν_i^{THEO}, which are used as the starting point for the numerical fitting (deconvolution) of the intervalence absorption to five Gaussian functions. The transition energies ν_i^{SPEC} resulting from this fitting are used for the first optimization of λ, H_{ab}, and modified ν_i^{THEO}. Subsequent iterations carried out by further (multiple) fittings to the experimental absorption envelope lead to the final optimized values of $\lambda = 5500$ cm^{-1} and $H_{ab} = 1900$ cm^{-1} and to the corresponding ν_i^{THEO}, listed in Table 4. The pictorial results of the digital simulation (see Table S3 for numerical parameters) are shown in Figure 7, which presents the five Gaussian components (in green), together with the fit of the composite spectrum (in red) to the experimental intervalence

Table 4. Calculated and Experimental Energies[a] and Relative Intensities[b] of Intervalence Optical Transitions in the Hexanuclear Cation-Radical **1c•+**

	$\Psi_1 \rightarrow \Psi_2$	$\Psi_1 \rightarrow \Psi_3$	$\Psi_1 \rightarrow \Psi_4$	$\Psi_1 \rightarrow \Psi_5$	$\Psi_1 \rightarrow \Psi_6$
theo[c]	3.7 (0.30)	4.8 (0.50)	7.5 (0.07)	8.6 (0.12)	10.1 ($\sim$0)
spec[d]	3.7 (0.25)	4.7 (0.52)	7.4 (0.10)	8.6 (0.13)	10.1 (0.01)

[a] In 10^3 cm^{-1}. [b] In parentheses, normalized intensities. [c] Calculated according to the six-state analysis with $\lambda = 5500$ cm^{-1} and $H_{ab} = 1900$ cm^{-1}.[30] [d] From the Gaussian deconvolution of the intervalence absorption band (Table S3 in the Supporting Information).

envelope (in black). The energies of the Gaussian components ν_i^{SPEC} and their normalized oscillator strengths are listed in Table 4.

It is important to note that, although the spectral fittings into five Gaussian bands provides the close correspondence ($R^2 > 0.999$) of the experimental and simulated spectra of **1c•+** and **1d•+** within a relatively wide range of $H_{ab} = 1600 \pm 400$ cm^{-1} and $\lambda = 5400 \pm 600$ cm^{-1},[52] we now apply two additional and independent criteria, i.e., (i) the band intensities and (ii) the redox potentials, to further validate the analysis, as follows.

(i) The *intensities* of the charge-transfer (intervalence) optical transitions are directly related to the corresponding transition moments, which can be expressed as $\mu_{oi} = \int\Psi_1\mu\Psi_i = \int(a_1\psi_a + ... + f_1\psi_f)\mu(a_i\psi_a + ... + f_i\psi_f) \approx (a_1a_i\mu_a + ... + f_1f_i\mu_f)$, where $i = 2$–6 and μ_a–μ_f are the moments of the diabatic states a–f within the arbitrarily chosen coordinate system. By setting the zero point of the coordinate system at the center of symmetry of the hexanuclear donor (i.e., in the center of the benzene ring), all vectors μ_a through μ_f can be expressed (based on symmetry reasons) as the product of the scalar constant μ and the unity vectors directed at 0, 60, 120, 180, 240, and 300° relative to the x-axes (taken as the direction from the benzene center to redox center "a").[53] Together with the coefficients (a_i–f_i) calculated with $\lambda = 5500$ cm^{-1} and $H_{ab} = 1900$ cm^{-1} (see Table S2), this leads to the striking correspondence between the

(51) Note that, generally speaking, the vibrational splittings of a single electronic transition could also lead to distinct components in the intervalence absorption spectrum. However, the intervalence spectra of cation-radicals **1c•+** and **1d•+** are much broader (and the separation between components larger) than in the spectrum for dinuclear cation-radical **5•+**, as previously observed in the NIR intervalence spectra of other dinuclear organic mixed-valence compounds showing vibrational splittings.[22c,d] Therefore, the vibrational splitting alone is unlikely to be sufficient to explain such a broadening of the spectra of **1c•+** and **1d•+**.

(52) Although it may seem, from the incompletely resolved spectra in Figure 7, that the digital deconvolutions are somewhat "overdetermined", we find that the three *independent* lines of unequivocal evidence provide the requisite (confirmative) information to more than offset any ambiguities. First, the unmistakable coincidences of the deconvolution results in Tables 4 and 6 with *all* the calculated energies as well as spectral intensities provide many ($\sim$20) fixed points to strongly support the validity of multistate analysis. Second, the calculated ground-state stabilizations based on these deconvolutions quantitatively accord with the *unique* electrochemical data presented in Table 5. Third, the multistate analysis carried out by digital deconvolution yields results that are equally applicable to aromatic arrays that are different, such as the dyad (**5•+**), the pentad (**6•+**), and the hexads (**1c•+** and **1d•+**).

(53) The calculated values of the transition moments (and therefore band intensities) do not depend on the choice of the coordinate system. For example, setting the zero point of the coordinate system at redox center a, the transition moment can be presented as $\mu_{oi} \approx a_1a_i\mu_a' + b_1b_i\mu_b' + ... + f_1f_i\mu_f' = a_1a_i(\mu_a - \mu_a) + b_1b_i(\mu_b - \mu_a) + ... + f_1f_i(\mu_f - \mu_a) = (a_1a_i\mu_a + b_1b_i\mu_b + ... + f_1f_i\mu_f) - (a_1a_i + b_1b_i + ... + f_1f_i)\mu_a = \mu_{oi}$ (the sum in the second set of parentheses is zero due to the orthogonality of states).
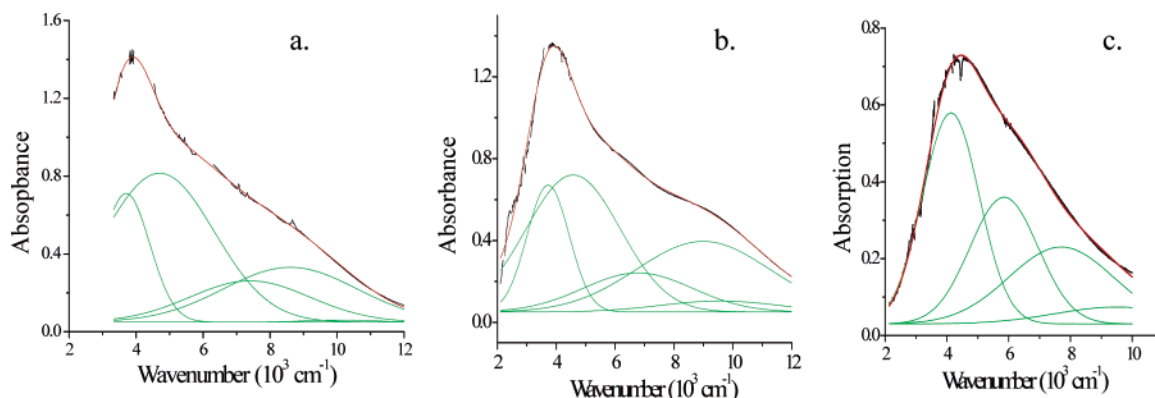
Figure 7. Spectral deconvolution of the NIR absorption bands for the hexanuclear cation-radicals $1c^{\bullet+}$ (a) and $1d^{\bullet+}$ (b) and the pentanuclear analogue $6^{\bullet+}$ (c), as described in the text.

Table 5. Resonance Stabilization (ΔG_r) of Cation-Radicals in Comparison with the Shift (δE)[b] of the First Oxidation Potential of Di- and Hexanuclear Donors Relative to That of Mononuclear Model **4**

cation-radical	ΔG_r, eV[a]	δE, V[b]
$5^{\bullet+}$	0.08	0.11
$1c^{\bullet+}$	0.15	0.23

[a] Calculated according to the two-state ($5^{\bullet+}$) or six-state ($1c^{\bullet+}$) analysis with $\lambda = 5500$ cm^{-1} and $H_{ab} = 1900$ cm^{-1}. [b] See Table 1.

Table 6. Calculated and Experimental Energies[a] and Relative Intensities[b] of Intervalence Optical Transitions in the Pentanuclear Cation-Radical $6^{\bullet+}$

	$\Psi_1 \rightarrow \Psi_2$	$\Psi_1 \rightarrow \Psi_3$	$\Psi_1 \rightarrow \Psi_4$	$\Psi_1 \rightarrow \Psi_5$
theo[c]	4.7 (0.40)	5.4 (0.31)	8.5 (0.23)	9.0 (0.06)
spec[d]	4.1 (0.39)	5.8 (0.28)	7.7 (0.26)	9.5 (0.07)

[a] In 10^3 cm^{-1}. [b] In parentheses, normalized intensities. [c] Calculated according to the five-state analysis with $\lambda = 5500$ cm^{-1} and $H_{ab} = 1900$ cm^{-1}. [d] From the Gaussian deconvolution of the intervalence absorption band.

calculated transition moments and the relative (normalized) intensities of each of the five transitions from the experimental (deconvoluted) values listed in Table 4.

(ii) *Voltammetric criteria* provide further support for the validity of our analysis. Thus, Table 5 presents the ground-state resonance stabilization (ΔG_r) of the cation-radicals of the dinuclear and hexanuclear donors, $5^{\bullet+}$, $1c^{\bullet+}$, and $1d^{\bullet+}$, relative to the mononuclear cation-radical $4^{\bullet+}$. The values in column 2 indicate that the resonance (ground-state) stabilization of hexanuclear cation-radicals is twice that of the dinuclear analogue (calculated with the same values of the reorganization energy λ and the coupling element H_{ab}).

Notably, such a stabilization represents the major component in the difference δE between the first oxidation potential of polynuclear donors and that of the mononuclear counterpart in column 3. (Note that $\delta E > \Delta G_r$ arises from the nonresonance contributions, such as entropy, electrostatic interactions, etc.[30,40]) Most importantly, the experimental (electrochemical) measurements of the oxidation potentials leads to $\delta E = 110$ mV for the dinuclear donor **5**, which is close to half that for the hexanuclear donor **1c** (230 mV). Thus, the observed doubling of the potential shift accords with changes in ΔG_r and, indeed, verifies the theoretical predictions of the multistate analysis.

III. Partial Electron Delocalization in the p-Doped Pentanuclear Donor. To further test the validity of the multistate analysis, let us also consider the spectral properties of the p-doped pentanuclear donor. Thus, the qualitative spectral comparison in Figure 3 shows that the spectrum of $6^{\bullet+}$ is intermediate between those of the dinuclear and the hexanuclear counterparts, being much broader and more red-shifted relative to the spectrum of $5^{\bullet+}$, but somewhat narrower and more blue-shifted relative to that of $1^{\bullet+}$. To apply the same multistate analysis, we take into account the fact that one of the six anilinyl groups (i.e., the methylated center) in cation-radical $6^{\bullet+}$ is excluded from the electron/hole delocalization. As such, the adiabatic wave functions must be now presented as the linear

combination of five diabatic wave functions. [The corresponding secular 5×5 determinant is presented in Chart S5 in the Supporting Information.] In this case, the electronic interaction of the methylated center with the neighboring anilinyl group must be excluded, and therefore the energetics of the system depends substantially on the placement of the hole. As such, we chose the placement of the hole on the group opposite to the methylated one (i.e., 0 should be in the center of the determinant to produce the lowest-energy ground state). The solution of this determinant, using the same values of $H_{ab} = 1900$ and $\lambda = 5500$ cm^{-1} as evaluated for the hexanuclear cation-radical, results in five adiabatic energy levels, with the corresponding coefficients describing the wave functions (Table S2). The solution leads to four electronic transitions with the energies and relative intensities presented in Table 6.
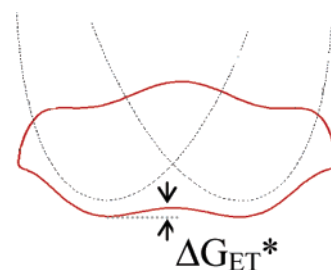
The main features of the theoretical prediction, i.e., the notable blue shift and the narrowing of the spectrum relative to that of the p-doped hexanuclear donor, agree with the experimental observations. Importantly, the parameters resulting from the digital deconvolution of the experimental spectrum (Figure 7c) also agree reasonably well with the calculated spectrum in Table 6, and these together provide the further important validation of the multistate analysis.

IV. Mechanism for Electron Migration in Various p-Doped Aromatic (Face-to-Face) Arrays. The diagnostic electronic spectra of the p-doped polynuclear donors presented in Figure 3 reveal two striking characteristics of the distinctive intervalence bands. First, the partially resolved near-IR bands all exhibit clear spectral maxima that are essentially invariant, with only slight (but regular) red shifts from the dinuclear $5^{\bullet+}$, to the pentanuclear $6^{\bullet+}$, and thence to the hexanuclear $1c^{\bullet+}$ and $1d^{\bullet+}$. Second, the nominal bandwidths (at half-maximum) of the same series of polynuclear cation-radicals show strong variations of 1500, 4000, and 5500 cm^{-1}, consistent with their digital deconvolutions into one,[37] four, and five Gaussian

components, respectively, in Figure 7. It is thus notable that the multistate analysis of these three types of intevalence absorption bands yields values of the reorganization energy and electronic coupling element that are the same within experimental error, with $\lambda = 5400 \pm 600$ cm^{-1} and $H_{ab} = 1600 \pm 400$ cm^{-1}, *irrespective of the number of redox centers.* As such, we now address the importance of the valid (theoretical) extension of the two-state analysis for the dyad $\mathbf{5}^{\bullet+}$ to the corresponding five-state analysis of the pentad $\mathbf{6}^{\bullet+}$ in Table 6 and to the six-state analysis of the hexad $\mathbf{1c}^{\bullet+}$ in Table 4. The simplest and most direct conclusion we can draw from the rather invariant values of λ and H_{ab} for all these p-doped polynuclear donors is that they share a common mechanism for electron migration that involves site-to-site electron hopping, the prototypical example of which is depicted by the potential-energy surface for the two-state dyad in Figure 6. As applied to the p-doped hexanuclear donors **1c** and **1d**, the evaluation of the potential energy surface for electron migration requires the extension of the single-point energy calculation (at $X = 0$[47a]) along the electron-transfer reaction coordinate. It should be stressed, however, that the traditional parabolic dependence of the diabatic (state) energy on the reaction coordinate is valid here only in limited segments of this multidimensional space. Therefore, as a first approximation, we consider electron transfer between two neighboring sites, a and b, as determined primarily by the parabolic dependence of the diabatic energies H_{aa} and H_{bb} on the nuclear coordinates of these two sites (as in the two-state analysis). We then assign $X = 0$ as described above, and $X = 1$ to the state with the hole on site b (with relaxed cationic geometry of this site and relaxed neutral geometry of site a). The electron hopping thus corresponds to movement from $X = 0$ to $X = 1$, with the transition state located at $X = 0.5$. Importantly, all other sites remain in the fixed nuclear geometry, and the energies of the other diabatic states are equal to λ at all points along this reaction coordinate. Accordingly, we determine the ground-state energy at different points from $X = 0$ to $X = 1$ for the six-state system in which the secular determinants include $H_{aa} = \lambda X^2$ and $H_{bb} = \lambda(1 - X)^2$, together with $H_{cc} = H_{dd} = H_{ee} = H_{ff} = \lambda$. The same procedure is applied to electron movement from site b to site c, etc. As a result, such a six-state analysis predicts the electron hopping along a hexagonal circuit, the closed potential-energy surface of which consists of six minima separated by the activation barriers[54] ΔG_{ET}^* as graphically depicted in the "roller coaster" topology shown in Chart 8.

V. Future Prospectives for Electron Interchange in p-Doped Cofacial Aromatic Arrays. For the *N,N*-diethyl- and methylethylanilinyl redox centers of principal focus in this study, the relevant values of $\lambda = 5400 \pm 600$ cm^{-1} and $H_{ab} = 1600 \pm 400$ cm^{-1} lead to the (averaged) activation barrier of $\Delta G_{ET}^* = 0.55 \pm 0.25$ kcal mol^{-1} for electron hopping from site to site.[54] To lower this barrier, we can imagine the synthesis of other multinuclear aromatic cation-radicals to modulate the relative electronic coupling and reorganization contributions in

---

(54) (a) Calculated with the six-state model as the difference between the minimum and the maximum ground-state energies on the electron-transfer reaction pathway from $X = 0$ to $X = 1$. (b) Thus, the multistate (temporal) events can be considered as a sequence of two-site processes in which the latter has been modified by the presence of four neighboring states. (c) It is interesting to speculate that the rate of such an electron (hole) migration in the manner of a "ring current" may be externally modulated by applied magnetic and/or electrostatic fields.

Chart 8

order to further lower the barrier and increase the electron-transfer rate. If so, at the upper limit of Class II systems at or close to the Class III border with $H_{ab} = \lambda/2$, the separate concepts of electron hopping versus π-delocalization are merged, and their distinction becomes obscure — an ambiguous situation aptly described by Nelsen as "almost delocalized".[9b] Indeed, such a conundrum is common in chemistry, and there are continuing polemics regarding the classical concepts of equilibrium versus resonance, valence-bond versus molecular-orbital, etc.[55]

The ultimate achievement of Class III and π-delocalization can be visualized with a *single ground state* for the three types of p-doped polynuclear aromatic arrays discussed in this study, as shown in Chart 9. In Chart 9, the blue-shaded areas represent

Chart 9
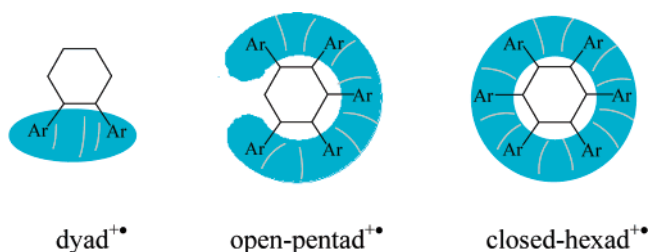
three-dimensional envelopes within which complete electron or charge delocalization occurs, i.e., (i) between both Ar redox centers in the dyad$^{\bullet+}$, (ii) among five contiguous redox centers in the open-pentad$^{\bullet+}$, and (iii) completely encompassing all redox centers of the hexad$^{\bullet+}$. Since such through-space interactions derive from juxtaposed face-to-face benzenoid rings,[6,28] π-delocalization is best described by (i) a short toroidal segment (dyad$^{\bullet+}$), (ii) an open toroid (open-pentad$^{\bullet+}$), or (iii) a full (donut-shaped) toroid (closed-hexad$^{\bullet+}$), as in Chart 9.[16] Indeed, they all represent the various extents of toroidal delocalization/ conjugation that is consonant with three-dimensional (multi-centered) interactions of cofacial aromatic moieties. The structural depiction of toroidal π-delocalization can also be applied in quantitative measure to intermolecular cofacial stacks of p-doped aromatic donors (as first presented in Chart 2 above) when these are considered as a linear combination of the diabatic reactant/product states. However, before proceeding much further, we emphasize the caveat that the theoretical treatment of electron transfer derived from the Mulliken–Hush analysis is semiempirical, and our quantitative evaluation of λ and H_{ab} in this study may not fully withstand more rigorous computations based on ab initio quantum-mechanical methodologies.

---

(55) (a) Hoffmann, R.; Shaik, S.; Hiberty P. S. *Acc. Chem. Res.* **2003**, *36*, 750. (b) Roberts, J. D. *Acc. Chem.* Res. **2004**, *37*, 417. (c) Streitwieser, A. *Acc. Chem. Res.* **2004**, *37*, 419.

Nonetheless, we believe the near coincidences of the experimental and theoretical results, as presented in Tables 4−6, all point strongly to the essential correctness of our principal conclusions regarding electron movement in various p-doped aromatic (cofacial) arrays. As such, we will continue our design of other new redox centers that will further facilitate electron interchange and eventually lead to Robin−Day Class III systems.

Experimental Section

Materials. *N*,*N*-Diethylaniline, potassium iodide, potassium iodate, phenylacetylene, acetylene, palladium chloride, triphenylphosphine, cuprous iodine, dicobalt octacarbonyl, lead dioxide, and tetraphenylcyclopentadienone (from Aldrich, Acros, or Alfa) were used as received. *N*-Methyl-*N*-ethylaniline and *N*-piperidinylaniline were synthesized according to the literature procedure,[56] and 4-iodo-*N*,*N*-dialkylaniline was prepared by iodination of *N*,*N*-dialkylaniline.[26] The dodecamethylcarborane radical was produced by oxidation of the cesium salt of decamethylcarboranate with PbO$_2$ in acetonitrile, followed by extraction with hexane.[33] Dichloromethane, toluene, diethylamine, dioxane, and tetrahydrofuran were purified according to published procedures.[57]

Syntheses. 1,2-Bis(*p*-*N*,*N*-diethylanilinyl)acetylene. Acetylene was bubbled into a stirred mixture of 4-iodo-*N*,*N*-diethylaniline (3.84 g, 14 mmol), PdCl$_2$ (30 mg), PPh$_3$ (90 mg), CuI (104 mg), and 60 mL of diethylamine at 40 °C. After 3 h, GC analysis showed complete consumption of 4-iodo-*N*,*N*-diethylaniline. The crude product, after removal of solvent, was purified by column chromatography (silica gel, hexane), and the light yellow crystalline 1,2-bis(*p*-*N*,*N*-diethylanilinyl)acetylene was obtained in 94% yield: mp 156−157 °C; ¹H NMR (CDCl$_3$) δ 7.35 (d, *J* = 8.7 Hz, 4H), 6.60 (d, *J* = 8.7 Hz, 4H), 3.36 (q, *J* = 6.9 Hz, 8H), 1.16 (t, *J* = 6.9 Hz, 12H); ¹³C NMR (CDCl$_3$) δ 146.9, 132.5, 111.2, 109.9, 87.8, 44.2, 12.5; MS (*m/e*) 321 (M$^+$ + 1, 40), 320 (M$^+$, 100), 305 (71), 281 (10), 276 (18), 261 (40). Anal. Calcd for C$_{22}$H$_{28}$N$_2$: C, 82.50; H, 8.75. Found: C, 82.36; H, 8.96.

1,2-Bis(*p*-*N*-methyl-*N*-ethylanilinyl)acetylene, 1-(*p*-*N*,*N*-diethylanilinyl)-2-phenylacetylene, and 1,2-bis(*p*-*N*-piperidinyl)acetylene were synthesized in a similar way. 1,2-Bis(*p*-*N*-methyl-*N*-ethylanilinyl)acetylene: mp 151−152 °C; ¹H NMR (CDCl$_3$) δ 7.35 (d, *J* = 8.7 Hz, 4H), 6.63 (d, *J* = 8.7 Hz, 4H), 3.41 (q, *J* = 6.9 Hz, 4H), 2.91 (s, 6H), 1.13 (t, *J* = 6.9 Hz, 6H); ¹³C NMR (CDCl$_3$) δ 146.9, 132.6, 111.9, 110.9, 88.1, 46.8, 37.6, 11.4; MS (*m/e*) 293 (M$^+$ + 1, 35), 292 (M$^+$, 100), 305 (71), 281 (10), 276 (18), 261 (40). Anal. Calcd for C$_{22}$H$_{28}$N$_2$: C, 82.19; H, 8.22. Found: C, 82.10; H, 8.25. 1,2-Bis(*p*-*N*-piperidinyl)acetylene: mp 157−158 °C; ¹H NMR (CDCl$_3$) δ 7.42 (d, *J* = 8.7 Hz, 4H), 6.95 (d, *J* = 8.4 Hz, 4H), 3.31 (t, *J* = 5.1 Hz, 8H), 1.72 (m, 8H), 1.66 (m, 4H); ¹³C NMR (CDCl$_3$) δ 133.7, 131.4, 116.6, 114.8, 88.4, 50.1, 26.0, 24.7. Anal. Calcd for C$_{24}$H$_{28}$N$_2$: C, 83.72; H, 8.14. Found: C, 83.77; H, 8.24. 1-(*p*-*N*,*N*-Diethylanilinyl)-2-phenylacetylene: yield 85%; mp 143−144 °C; ¹H NMR (CDCl$_3$) δ 7.35 (d, *J* = 8.7 Hz, 4H), 6.60 (d, *J* = 8.7 Hz, 4H), 3.36 (q, *J* = 6.9 Hz, 8H), 1.16 (t, *J* = 6.9 Hz, 12H); MS (*m/e*) 250 (M$^+$ + 1, 13), 249 (M$^+$, 75), 234 (100), 205 (17), 176 (15). Anal. Calcd for C$_{18}$H$_{14}$N: C, 86.56; H, 7.63. Found: C, 88.68; H, 7.66.

(*p*-*N*,*N*-Diethylanilinyl)pentaphenylbenzene (4). A mixture of 1.25 g (5 mmol) of 1,2-bis(*p*-*N*,*N*-diethylanilinyl)acetylene and 1.92 g (5 mmol) of tetraphenylcyclopentadienone was sealed in a glass tube and heated at 200 °C for 24 h. The reaction mixture was purified by column chromatography (silica gel, hexane/CH$_2$Cl$_2$, 80/20) to give 2.3 g of white crystalline **4**: yield 76%; mp > 250 °C; ¹H NMR (CDCl$_3$) δ 6.86−6.83 (m, 25H), 6.59 (d, *J* = 8.4 Hz, 2H), 6.22 (d, *J* = 8.4 Hz, 2H), 3.13 (q, *J* = 6.9 Hz, 2H), 0.96 (t, *J* = 6.9 Hz, 2H); ¹³C NMR

(56) Adimurthy, S.; Ramachandraiash, G.; Ghosh, P. K.; Bedekar, A. V. *Tetrahedron Lett.* **2003**, *44*, 5099.
(57) Perrin, D. D.; Armarego, W. L. F.; Perrin, D. R. *Purification of Laboratory Chemicals,* 2nd ed.; Pergamon: New York, 1980.

(CDCl$_3$) δ 145.2, 141.0, 140.8, 140.7, 140.5, 140.2, 140.0, 132.1, 131.5, 131.4, 128.1, 126.4, 124.9, 124.7, 111.5, 44.1, 12.1. Anal. Calcd for C$_{46}$H$_{39}$N: C, 91.24; H, 6.45. Found: C, 91.22; H, 6.48.

1,2-Bis(*p*-*N*,*N*-diethylanilinyl)tetraphenylbenzene (5) was synthesized in a similar way: yield 25%; mp > 250 °C; ¹H NMR (CDCl$_3$) δ 7.80 (m, 20H), 6.63 (d, *J* = 8.7 Hz, 4H), 6.27 (d, *J* = 8.7 Hz, 4H), 3.15 (q, *J* = 6.9 Hz, 8H), 0.97 (t, *J* = 6.9 Hz, 12H); ¹³C NMR (CDCl$_3$) δ 145.1, 141.3, 141.0, 140.8, 140.3, 139.5, 132.3, 131.6, 131.5, 128.9, 126.4, 124.8, 124.6, 111.8, 111.4, 44.3, 12.1. Anal. Calcd for C$_{50}$H$_{48}$N$_2$: C, 88.76; H, 7.10. Found: C, 88.74; H, 7.15.

Hexakis(*p*-*N*,*N*-diethylanilinyl)benzene (1c). A 2.4 g portion of 1,2-bis(*p*-*N*,*N*-diethylanilinyl)acetylene and 100 mg of dicobalt octacarbonyl were dissolved in 30 mL of dioxane, and the mixture was heated at reflux for 2 days. Solvent was then removed, and the mixture was purified by column chromatography to yield 1.32 g of **1c**: yield 55%; mp > 250 °C; ¹H NMR (CDCl$_3$) δ 6.62 (d, *J* = 8.4 Hz, 12H), 6.28 (d, *J* = 8.4 Hz, 12H), 3.12 (q, *J* = 6.9 Hz, 24H), 0.95 (t, *J* = 6.9 Hz, 36H); ¹³C NMR (CDCl$_3$) δ 144.7, 140.2, 132.6, 130.5, 112.3, 44.6, 12.1. Anal. Calcd for C$_{66}$H$_{84}$N$_6$: C, 82.50; H, 8.75. Found: C, 82.34; H, 8.67.

Hexanuclear donors **1a**, **1b**, and **1d** were obtained by the same procedure, starting with the corresponding acetylene precursors. Hexakis-1,2-bis(*p*-*N*-piperidinylanilinyl)benzene (**1a**): yield 50%; mp > 250 °C; ¹H NMR (CDCl$_3$) δ 6.70 (d, *J* = 8.4 Hz, 12H), 6.54 (d, *J* = 6.9 Hz, 12H), 3.03 (t, *J* = 5.1 Hz, 24H), 1.69 (m, 24H), 1.59 (m, 12H); ¹³C NMR (CDCl$_3$) δ 149.3, 140.7, 133.8, 131.6, 114.6, 51.4, 26.1, 24.8. Anal. Calcd for C$_{72}$H$_{84}$N$_6$: C, 83.72; H, 8.14. Found: C, 83.88; H, 8.14. Hexakis(*p*-*N*,*N*-di-*p*-bromophenylanilinyl)benzene (**1b**): yield 15%; mp > 250 °C; ¹H NMR (CDCl$_3$) δ 7.27 (d, *J* = 7.8 Hz, 24H), 6.77 (m, 48H); ¹³C NMR (CDCl$_3$) δ 146.4, 144.6, 140.1, 132.8, 132.5, 125.4, 123.6, 115.5. Hexakis(*p*-*N*-methyl-*N*-ethylanilinyl)benzene (**1d**): yield 58%; mp > 250 °C; ¹H NMR (CDCl$_3$) δ 6.62 (d, *J* = 8.4 Hz, 12H), 6.28 (d, *J* = 8.4 Hz, 12H), 3.18 (q, *J* = 6.9 Hz, 12H), 2.69 (s, 18H), 0.93 (t, *J* = 6.9 Hz, 18H); ¹³C NMR (CDCl$_3$) δ 146.2, 140.5, 132.7, 122.5, 112.2, 47.5, 37.7, 10.5. Anal. Calcd for C$_{66}$H$_{84}$N$_6$: C, 82.19; H, 8.225. Found: C, 82.22; H, 8.25.

Hexakis(*N*-3,6-di-*n*-butoxylcarbazolyl)benzene (2). 3,6-Di-*n*-butoxylcarbazole (504 mg, 1.74 mmol) was added to 84 mg (1.75 mmol) of NaH (50%) and stirred under argon at room temperature in 5 mL of DMF. After 30 min, 53.9 mg (0.29 mmol) of hexafluorobenzene was added, and the mixture was stirred for an additional 3 h. The mixture was poured into 100 mL of water, and the white precipitate (290 mg) was filtered and dried; its X-ray crystallographic analysis (Figure S5 in the Supporting Information) revealed that it is 1,2,4,5-(*N*-3,6-di-*n*-butoxylcarbazolyl)-3,6-fluorobenzene. This precipitate was added to the potassium salt of carbazole (prepared by the addition of 28 mg of potassium metal to 223 mg of 3,6-di-*n*-butoxylcarbazole) in 5 mL of HMPA, and the mixture was stirred at 90 °C overnight. After cooling, the mixture was poured into 50 mL of water and extracted with dichloromethane (3 × 30 mL). The organic extract was washed with water (3 × 30 mL) and dried over MgSO$_4$. The solvent was removed, and the residue was recrystallized from CH$_2$Cl$_2$/MeOH to give 218 mg of **2** as a white crystalline product (Figure 1C): ¹H NMR (CDCl$_3$) δ 6.88 (d, *J* = 7.8 Hz, 12H), 6.72 (d, *J* = 2.1 Hz, 12H), 6.17 (dd, *J* = 7.8, 2.1 Hz, 12H), 3.73 (t, *J* = 6.6 Hz, 24H), 1.67 (m, *J* = 7.2 Hz, 24H), 1.39 (m, *J* = 7.2 Hz, 24H), 0.92 (t, *J* = 7.2 Hz, 36H); ¹³C NMR (CDCl$_3$) δ 153.0, 135.8, 133.8, 124.0, 113.6, 111.3, 103.6, 68.4, 31.4, 19.2, 13.9.

Pentanuclear Donor (*N*,*N*-Dimethyl-*N*-ethylammonium-4′-phenyl)-penta(*N*-ethyl-*N*-methylanilinyl)benzene Triflate Salt (6·OTf). A 48 μL aliquot of methyl triflate (0.43 mmol) was added to 745 mg (0.85 mmol) of **1b** in 20 mL of dichloromethane, and the solution was stirred at room temperature overnight. The reaction mixture was purified by column chromatography over silica gel with CH$_2$Cl$_2$/acetone (20:1) to recover 400 mg of **1b**, and then it was eluted with acetone to obtain 330 mg of **6·OTf** (as triflic acid solvate) as a white solid: yield 80%

(based on methyl triflate added); mp > 250 °C; ^{1}H NMR (acetone) δ 7.60 (d, J = 7.8 Hz, 12H), 6.72 (d, J = 2.1 Hz, 12H), 6.17 (dd, J = 7.8 Hz, 2.1 Hz, 12H), 3.73 (t, J = 6.6 Hz, 24H), 1.67 (m, J = 7.2 Hz, 24H), 1.39 (m, J = 7.2 Hz, 24H), 0.92 (t, J = 7.2 Hz, 36H); ^{13}C NMR (CDCl$_3$) δ 153.0, 135.8, 133.8, 124.0, 113.6, 111.3, 103.6, 68.4, 31.4, 19.2, 13.9. Anal. Calcd for C$_{62}$H$_{75}$F$_3$N$_6$O$_3$S·0.85CF$_3$SO$_3$H: C, 64.39; H, 6.54. Found: C, 64.50; H, 6.43.

Isolation of Cation-Radical Salts of p-Doped Polynuclear Donors. Typically, to prepare a p-doped cation-radical salt, 3.2 mL of a 15.6 mM solution of **CB**• was added to a stirred solution of 48 mg (0.05 mmol) of hexanuclear donor **1c** in 2 mL of dichloromethane at −60 °C. The dark-blue solution was stirred for 30 min, and then 6 mL of hexane was added. The resulting dark-blue precipitate was filtered, washed with hexane (2 × 2 mL), and dried in vacuo. The isolated solid powder (57 mg) corresponded to a 90% yield of **1c**•+ **CB**−, and its purity was established to be 97% by spectral titration with *p*-chloranil anion-radical (oxidation potential of ~0 V vs SCE) as follows. A 1 mM solution of NPr$_4^+$ *p*-CA•− in dichloromethane was added incrementally to the stirred solution of **1c**•+ **CB**− (13 mg, 0.01 mmol) in 1 mL of dichloromethane until the solution became colorless. In two separate experiments, 9.8 and 10.1 mL amounts of the solution of *p*-chloranil were consumed until the blue color of **1c**•+ disappeared, which corresponded to 98% and 101% purity of the dark-blue solid **1c**•+ **CB**−. In the same manner, the solid dark-blue powders of **4**•+ **CB**− and **5**•+ **CB**− were prepared in 88% and 80% yields, respectively, starting with the corresponding mono- and dinuclear donors **4** and **5**; the purities of the salts were found by titration with *p*-chloranil to be 99% and 98%, respectively. Similarly, 5 mL of a 2 mM solution of **CB**• was added to 10.4 mg of **6**·OTf dissolved in 1 mL of dichloromethane at −68 °C. The titration of the resulting dark-blue solution with the p-chloranil anion-radical indicated 90% yield of the dication-radical **6**•+.

Instrumentation. The ^{1}H NMR spectra were recorded on a General Electric QE-300 NMR spectrometer, and the chemical shifts are reported in ppm downfield from internal tetramethylsilane. UV−NIR spectra were measured with a Varian Cary 500 spectrometer, and infrared spectra were recorded on a Nicolet 10 DX FT spectrometer. GC−MS analyses were carried out on a Hewlett-Packard 6890A (G1530A) chromatograph with a HP5973 Network mass-selective detector. Cyclic voltammetry (CV) and Osteryoung square-wave voltammetry (OSWV) were performed on a BAS 100A electrochemical analyzer, and the ESR spectra were measured with a Varian E-line Century Series ESR spectrometer as described previously.[6] X-ray crystallographic measurements were performed with a Bruker SMART diffractometer equipped with a 1K CCD detector using Mo Kα radiation (λ = 0.71073 Å) at −150 °C. The structures were solved by direct methods and refined by the full-matrix least-squares procedure;[58] the X-ray structure details are on deposit and can be obtained from the Cambridge Crystallographic Database.

Calculation of the Equilibrium Concentrations of Different Oxidation States of Polynuclear Donors. The redox equilibria in solutions of hexanuclear donors **1** upon addition of **CB**• can be presented as

$$\mathbf{1}^{(n-1)+} + \mathbf{CB}^\bullet \rightleftarrows \mathbf{1}^{n+} + \mathbf{CB}^- \tag{9}$$

where n = 1−6. The equilibrium concentrations of $\mathbf{1}^{n+}$, **CB**•, and **CB**− are related via the set of equations

$$K^n = [\mathbf{1}^{n+}][\mathbf{CB}^-]/[\mathbf{1}^{(n-1)+}][\mathbf{CB}^\bullet] \tag{10}$$

where K^n is the equilibrium constant determined by the redox potential differences,

$$K^n = S \exp((E_{red} - E_{1/2}{}^n)F/RT) \tag{11}$$

E_{red} is the reduction potential of the carborane radical, $E_{1/2}{}^n$ is the oxidation potential of the $(n-1)^+$ to n^+ oxidation states of the hexanuclear donors (Table 1), and S is the entropy-related factor.[59] On the basis of eq 10 (with the equilibrium constants calculated via eq 11), and taking into account the mass balance, i.e., $\sum[\mathbf{1}^{n+}] = [\mathbf{1}]_o$, and the charge balance, i.e., $\sum n[\mathbf{1}^{n+}] = [\mathbf{CB}^\bullet]_o + [\mathbf{CB}^-]$ ($n = 1{-}6$), the equilibrium concentrations of all the components were numerically calculated with the Mathematica program.[48] The dependence of the concentration of each oxidation state on the concentration of the oxidant added to the solution is presented in Figure 4.

Spectral Titration of Polynuclear Donors. The UV−vis−NIR absorption spectra were recorded at −20 °C in a Dewar equipped with a quartz lens, using a quartz spectroscopic cell with a 1-mm path length and equipped with a Teflon valve fitted with Viton O-rings. Typically, a 1 mM solution of the neutral donor **1** (or pentanuclear cation **6**) was prepared in a Schlenk tube and transferred under argon into the spectroscopic cell. The oxidant **CB**• was added to this solution so that the ratio of concentrations of carborane radical to donor varied from 0.1:1 to 10:1. [To ensure reproducibility, fresh solutions of **1** or **6** were used in each measurement.] Upon the addition of oxidant, the colorless solution immediately turned blue, and the spectrum was recorded. Spectra of the solutions with oxidant/donor ratios varying from 0:1 to 2:1 are shown in Figure 5 and described in the text. Further increases of oxidant (beyond a 2:1 ratio) led to a decrease of the intensity of the band at λ_{max} = 1530 nm, which indicated that higher oxidation states did not absorb significantly in the near-IR range (see Figure S3 in the Supporting Information).

Among the various hexaarylbenzenes examined, the *N,N*-dialkylanilinyl analogues showed the most significant splitting of the CV waves, with a clear separation of the first oxidation wave and the broadest NIR absorption. By comparison, the oxidation of hexakis(*p*-bromophenylanilinyl)benzene **1b** with **CB**• contained only a small fraction of cation-radical **1b**•+ (within a single CV wave, the distribution among oxidation states is determined by statistical factors). The electronic spectrum of this solution showed a local band (characteristic of the mononuclear analogue), together with a NIR absorption with λ_{max} = 1500 nm (Figure S6), that could be related to a mixture of mono- and dications (since the 3+ to 6+ oxidation states of donors **1c**, **1d**, and **6** have relatively weak absorptions in the NIR range). The ESR spectrum of this solution consisted of 13 lines, with a hyperfine splitting constant of a_N = 1.7G (Figure S7) and $\langle g \rangle$ = 2.0030. Comparison with the ESR spectrum of the mononuclear triphenylamine cation-radical (characterized by hyperfine nitrogen splittings of ~10 G[60]) suggested that this splitting was related to fast spin delocalization over six nitrogen centers. Thus, the CV data point to a relatively weak interaction between the redox centers in **1b**•+, which may be related to partial charge delocalization onto the *p*-bromophenyl substituents. However, the interaction is probably still sufficient to ensure fast (on the ESR time scale) charge migration between the redox sites.

Likewise, the oxidation of the carbazole-based hexanuclear donor **2** led to the appearance of the local absorption in the visible region and an additional NIR band with λ_{max} = 1310 nm. Essentially the same spectral shape was obtained when the tetracarbazole derivative was oxidized. This indicated that the NIR absorptions in such polynuclear cations derived from only the pairwise interaction of redox centers (Figure S8). The ESR spectrum consisted of one broad, unresolved peak with $\langle g \rangle$ = 2.0028, and was independent of the temperature (+22 to −88 °C). The spectral (UV−vis−NIR and ESR) characterization of

(58) (a) Sheldrick, G. M. *SADABS*, Version 2.03; Bruker/Siemens Area Detector Absorption and Other Corrections, 2000. (b) Sheldrick, G. M. *SHELXS 97*, Program for Crystal Structure Solutions; University of Göttingen: Göttingen, Germany, 1997. (c) Sheldrick, G. M. *SHELXL 97*, Program for Crystal Structure Refinement; University of Göttingen: Göttingen, Germany, 1997.

(59) S = 1, 6, 15, 20, 15, 6, and 1 for the 0 to +6 oxidation states, respectively.
(60) Van Willigen, H. *J. Am. Chem. Soc.* **1967**, *89*, 2229.

p-doped hexapyrrole donor **3** suffered from its cation-radical instabilities, even at low temperature, since the solution of this donor bleached immediately upon the addition of carborane oxidant, even at -78 °C.

X-ray Crystallography of Hexanuclear Donors. Single crystals were prepared by slow evaporation of solvent from the solutions of hexanuclear donors in a CH_2Cl_2/CH_3CN mixture. **1c:** formula, $C_{66}H_{84}N_6\cdot0.09CH_2Cl_2$; MW, 968.36; triclinic, space group $P\bar{1}$; $a = 9.3616(6)$, $b = 18.615(1)$, and $c = 18.893(1)$ Å; $\alpha = 63.621(1)$, $\beta = 84.051(1)$, and $\gamma = 78.052(1)°$; $V = 2885.4(3)$ Å^3; $Z = 2$; $\rho = 1.115$ g cm^{-3}. The total number of reflections measured at 123 K was 26 797, of which 14 246 were symmetrically nonequivalent. Final residuals were $R1 = 0.0984$ and w$R2 = 0.2957$ for 10 392 reflections with $I > 2\sigma(I)$. **1d:** formula, $C_{60}H_{72}N_6\cdot2CH_2Cl_2$; MW, 1047.09; triclinic, space group $P\bar{1}$; $a = 9.750(4)$, $b = 15.374(6)$, and $c = 19.369(11)$ Å; $\alpha = 96.84(3)$, $\beta = 95.38(4)$, and $\gamma = 90.80(3)°$; $V = 2869(2)$ Å^3; $Z = 2$; $\rho = 1.212$ g cm^{-3}. The total number of reflections measured at 173 K was 42 791, of which 16 456 were symmetrically nonequivalent. Final residuals were $R1 = 0.0782$ and w$R2 = 0.2304$ for 5945 reflections with $I > 2\sigma(I)$. **2:** formula, $C_{126}H_{135}N_6O_{12}\cdot4C_2H_3N$; MW, 2089.62; monoclinic, space group $C2/c$; $a = 39.292(2)$, $b = 116.3439(9)$, and $c = 40.408(2)(11)$ Å; $\beta = 111.055(2)°$; $V = 24217(2)$ Å^3; $Z = 8$; $\rho = 1.146$ g cm^{-3}. The total number of reflections measured at 123 K was 130 050, of which 21 554 were symmetrically nonequivalent. Final residuals were $R1 = 0.0626$ and w$R2 = 0.177$ for 8870 reflections with $I > 2\sigma(I)$.

Computational methodology for the Mulliken−Hush analysis of the pentanuclear cation-radical **6$^{•+}$** and the hexanuclear cation-radicals **1c$^{•+}$** and **1d$^{•+}$** is described in the Supporting Information.

Supporting Information Available: CV and OSWV of donors **1a**, **1b**, and **2** and the tetracarbazolyldifluorobenzene derivative (Figure S1); ESR spectrum of monoanilinyl donor **4$^{•+}$** (Figure S2); electronic spectra of the higher oxidation states of hexanuclear donor **1c** (Figure S3); electronic spectra of the higher oxidation states of pentanuclear donor **6** (Figure S4); ORTEP diagram of tetracarbazolyldifluorobenzene (Figure S5); electronic spectrum of oxidation products of donor **1b** (Figure S6); ESR spectrum of **1b$^{•+}$** (Figure S7); electronic spectra of the oxidation products of hexa- and tetracarbazolylbenzene derivatives (Figure S8); electronic spectra of cation-radicals in the NIR and IR range (Figure S9); electronic spectrum of the cation-radical **5$^{•+}$** in the vis−NIR range (Figure S10); solution of the six-state determinant (Charts S1−S4 and Table S1); solution of the five-state determinant (Chart S5 and Table S2); parameters for the Gaussian deconvolution for **1c$^{•+}$** and **6$^{•+}$** (Table S3); and details of the multistate analysis. This material is available free of charge via the Internet at http://pubs.acs.org.

JA060393N